ANNUAL STATUS REPORT

NASA Grant NAGW-3001

February 23, 1993

TITLE PAGE

Type of Report ..... Annual Status Report
Period Covered ..... May 1, 1992 — February 28, 1993
Grant Number NAGW-3001
Title of Grant ..... "Theory of Grain Alignment in Molecular Clouds"
Principal Investigator ..... Dr. Wayne G. Roberge
Grantee's Address ..... Physics Dept.
..... Rensselaer Polytechnic Institute
..... Troy, NY 12180-3590

REPORT ON THE PERIOD MAY 1, 1992 — FEBRUARY 28, 1993

A. Research Accomplishments

I am pleased to report that we have greatly exceeded the original goals for the first year of this project.

1. Mathematical Theory of Grain Alignment

We have formulated a new mathematical technique for predicting grain alignment and polarization in molecular clouds. The new technique is completely general, in the sense that it can be used to calculate the efficiency of any alignment mechanism. It computes the "Rayleigh reduction factor," R,[1] by numerically integrating the "Langevin equation for Brownian rotation." An algorithm for solving the Langevin equation has been developed and thoroughly debugged via benchmark calculations on special cases where exact analytic solutions for R exist. The benchmark tests show that we are able to calculate R accurate to typically 2% (3σ error) and that any systematic errors which may be present in our calculations correspond to spurious predictions of alignment which are well below the limits of detectability. We have implemented our algorithm on a parallel-processing machine with 2048 independent processors. Consequently, we now have the capacity to produce more results in one month than the combined results of all previously published work on grain alignment theory! This work has been submitted for publication.

2. Super-Paramagnetic Alignment of Molecular Cloud Grains

Before this project was funded, no calculations existed which could be used to compare near- and far-infrared polarimetric observations with the predictions of one theory— super-paramagnetic relaxation— which is generally considered to be a viable model for grain alignment in molecular clouds. We have carried out such calculations. The grains were modeled as refractory cores with ice mantles, where the core and mantle surfaces were represented as confocal, oblate spheroids of arbitrary eccentricity. We included a proper treatment of the Barnett effect, rotational anelasticity, Larmor precession, gas-grain collisions, thermal evaporation of molecules from the mantle surface, super-paramagnetic absorption, and thermal fluctuations in the grain magnetization. We developed and incorporated a quantitative theory for the effects of thermal emission and infrared absorption on the alignment of nonspherical grains. We also carried out an exhaustive numerical study of the super-paramagnetic alignment scenario. Our calculations show that super-paramagnetic alignment, in the absence of suprathermal rotation, is *not* consistent with the degree of alignment inferred by Lee and Draine (1985, ApJ, 290, 211) from an analysis of infrared extinction and polarimetry for the line of sight toward the BN object. This conclusion is independent of any assumptions about the uncertain grain magnetic properties. Our results were presented at the January, 1993 AAS meeting and a related paper will be submitted for publication before May 1. Calculations for another paper, on the analogous effects for *prolate* spheroids, are in progress.

3. Theory of Grain Alignment by Ambipolar Diffusion

The differential motion of ions and neutral particles in a partially-ionized plasma is called "ambipolar diffusion." A charged grain in such a plasma will also drift through the neutrals, with a gas-grain drift speed, v_d, determined by the balance between the Lorentz and gas drag forces on the grain. Furthermore, if v_d is comparable to the gas thermal speed, then the grains will become aligned by a process known as "Gold's mechanism." Gas-grain drift at thermal speeds is predicted in recent theoretical models of protostars (by Mouschovias and collaborators) and the neutral gas ring at the Galactic center (by Wardle and Königl). *It follows that grain alignment and polarization are implicit predictions of these models which can be used to test their validity.*

One of our first-year goals was the development of a quantitative theory for grain alignment by ambipolar diffusion. Such a theory has now been developed by us for spherical grains. An *exact* analytic solution has been found for the alignment of spheres subject to the effects of ambipolar diffusion plus paramagnetic or super-paramagnetic absorption and the other processes listed in item 1 above. This solution has been

[1] The Rayleigh reduction factor is a statistic of the grain angular momentum distribution which measures the efficiency of alignment.

used, in conjunction with a model for the grain optical properties, to generate theoretical predictions of the polarized, far-infrared emission from warm grains in a gas undergoing ambipolar diffusion. Our calculations show that detectable linear polarizations ($\approx 1 - 5\%$) can be produced by this mechanism. A paper on the basic physics of these processes will be submitted before May 1. Our results will be applied in Year 2 to calculate the far-infrared polarization which is predicted implicitly by the Wardle-Königl models of the Galactic center gas ring. These predictions will be compared with far-infrared polarimetry of the ring by Hildebrand and collaborators, thereby testing the Wardle-Königl models.

4. Publications

Roberge, W.G., DeGraff, T.A., and Flaherty, J.E. 1993, "The Langevin Equation and its Application to Grain Alignment in Molecular Clouds," submitted to ApJ.

Roberge, W.G., DeGraff, T.A., and Flaherty, J.E. 1992, "Super-Paramagnetic Alignment of Core-Mantle Grains," BAAS, vol. 24, no. 4, p. 1121 (abstract).

DeGraff, T.A., Roberge, W.G., and Flaherty, J.E. 1993, "Magnetic Grain Alignment in Molecular Clouds," to be submitted before May 1, 1993.

Roberge, W.G., Hanany, S., and Messinger, D. 1993, "Grain Alignment by Ambipolar Diffusion," to be submitted before May 1, 1993.

B. Summary of Expenditures

Item	Budget	Actual
PI Summer Salary	$5,954	$0
Grad Student Tuition	4,417	5,736
Grad Student Academic Yr. Salary	4,600	9,200
Grad Student Summer Salary	3,220	6,398
Typing and Clerical Assistance	350	353
Fringe Benefits	1,324	74
Travel (domestic)	1,200	1,251
Computer Usage	2,000	2,000
Publication Costs/Page Charges	1,500	38
Communications	175	163
Indirect Costs	10,260	9,787
Totals	**$35,000**	**$35,000**

Differences between the actual and budgeted expenditures were due to the following:

- The graduate student (Trudy DeGraff) had to be supported for a full year, not half a year as planned. To cover the increase in grad student support, the PI did not pay himself summer salary. This had no effect on the PI's level of commitment to the project and he did not receive summer salary from any other sources.
- The PI supported 2 grad students during summer, 1992 instead of one. DeGraff worked on the mathematical theory of grain alignment and David Messinger worked on the theory of grain alignment by ambipolar diffusion.
- The page charges for Paper 1 have not been billed at this date.

THE LANGEVIN EQUATION AND ITS APPLICATION TO GRAIN ALIGNMENT IN MOLECULAR CLOUDS

W. G. Roberge

Physics Dept., Rensselaer Polytechnic Institute, Troy, NY 12180-3590

T. A. DeGraff and J. E. Flaherty

Dept. of Computer Science, Rensselaer Polytechnic Institute, Troy, NY 12180-3590

Submitted to the *Astrophysical Journal*

ABSTRACT

We describe a new computational method for solving problems in grain alignment theory which uses numerical integration of the Langevin equation for Brownian rotation. The new method is completely general in the sense that it generates the solution to a Fokker-Planck equation with arbitrary diffusion coefficients. We derive accurate expressions for the diffusion coefficients of refractory grains with ice mantles, on the *ad hoc* hypothesis that the grains rotate with thermal kinetic energies. We include the effects of internal dissipation by Barnett relaxation or rotational anelasticity, Larmor precession, gas-grain collisions, thermal evaporation, and paramagnetic or super-paramagnetic absorption. We develop a quantitative theory for the effects of thermal emission and infrared absorption on the alignment of nonspherical grains and assess the relevance of these processes to polarization in molecular clouds. We document the accuracy of our computational method by comparing numerical solutions for the Rayleigh reduction factor of magnetically aligned grains with exact solutions for spheres and thin disks.

Subject headings: polarization — interstellar: grains

1 INTRODUCTION

Interstellar polarization is intimately related to the rotational dynamics of dust grains. Observational evidence shows unambiguously that, in both atomic and molecular regions of the interstellar medium, polarization by dust is caused by nonspherical grains whose axes are partially aligned with respect to $\boldsymbol{B}$, the ambient magnetic field (e.g., Whittet 1992). Because the direction of each grain's angular momentum vector, $\boldsymbol{J}$, is tightly correlated with the direction of the grain's principal axis of largest rotational inertia (Purcell 1979 [P79], see also §3.4), the polarimetric observations imply further that $\boldsymbol{J}$ must be partially aligned with respect to $\boldsymbol{B}$. Thus, "grain alignment" means "angular momentum alignment." It can be shown (Lee & Draine 1985) that the degree of linear or circular polarization from a cloud of dust depends on the grain angular momentum distribution only via the "Rayleigh reduction factor,"

$$R \equiv \frac{3}{2}\left[\left\langle \cos^2\beta \right\rangle - \frac{1}{3}\right] \tag{1.1}$$

(Greenberg 1968), where β is the angle between $\boldsymbol{J}$ and $\boldsymbol{B}$ and the angle brackets denote the average over an ensemble of identical grains. Thus, the Rayleigh reduction factor characterizes the degree of alignment, with R varying from zero for an isotropic angular momentum distribution to unity for a distribution with $\boldsymbol{J}$ perfectly aligned parallel to $\boldsymbol{B}$. All observations of polarized extinction and emission by dust are presently consistent with $R > 0$, i.e., with the alignment of $\boldsymbol{J}$ preferentially parallel rather than normal to $\boldsymbol{B}$ (Hildebrand 1989; Whittet 1992).

Grain alignment theory is a problem in statistical mechanics, the object of which is to predict the angular momentum distribution and thus R in terms of the various torques which act upon the grains. It is a remarkable fact that, more than forty years after the discovery of interstellar polarization, a convincing theory of the alignment mechanism remains to be established. While several physical processes are known which produce torques of the right type to align the grains (see the reviews by Hildebrand 1988a,b), it is unclear whether any of the processes which have been studied extensively can overcome the disalignment of $\boldsymbol{J}$ by random gas-grain collisions. For example, alignment by paramagnetic torques as described in

the classical Davis-Greenstein mechanism (Davis & Greenstein 1951 [DG]) can be ruled out unequivocally in H I clouds (Spitzer 1978; Whittet 1992) and at least some molecular clouds (Jones, Hyland, & Bailey 1984; Lee & Draine 1985). Similarly, it is difficult to reconcile the near-ubiquity of interstellar polarization with alignment either by gas-grain streaming (Gold 1952; Purcell 1969), or by anisotropic radiation fields (Harwit 1970), both of which require rather special physical conditions. However, two variants of the classical DG mechanism may plausibly explain both the H I and molecular cloud observations (Hildebrand 1989): Magnetic alignment is greatly enhanced if the grains contain small ferromagnetic inclusions, thereby increasing the aligning torque to "super-paramagnetic" values (Spitzer & Tukey 1951; Jones & Spitzer 1967 [JS67]; Purcell & Spitzer 1971 [PS71]; Duley 1978). Alternatively, or perhaps in conjunction with super-paramagnetism, the grains may rotate at suprathermal kinetic energies, thereby rendering $\boldsymbol{J}$ impervious to disalignment by gas-grain collisions (Purcell 1979 [P79], Spitzer & McGlynn 1979; Johnson et al. 1981; Johnson 1982). At present, however, observational evidence regarding the super-paramagnetism and/or suprathermal rotation of interstellar grains is inconclusive (Hildebrand 1989). An unfortunate consequence of the ambiguous cause of grain alignment is that the relation between the polarization-to-extinction ratio and magnetic field strength in clouds is unknown.

The wealth of polarimetric data which have been acquired from molecular cloud observations during the past decade may provide important clues to the resolution of this problem. For example, polarization is observed in cold, quiescent globules where the dust-to-gas temperature ratio, T_d/T_g, is known to be close to unity (e.g., Jones et al. 1984). It is possible that these observations are inconsistent with super-paramagnetic alignment, which vanishes in the limit $T_d/T_g \longrightarrow 1$ unless the grains are also rotating suprathermally. Unfortunately, however, there is presently no way to assess this possibility, because there are no theoretical predictions on super-paramagnetic alignment in the absence of suprathermal rotation which can be compared with the observations. In particular, the last extensive calculations (PS71) preceded the discovery of physical processes (Dolginov & Mytrophanov 1976; P79) which affect the grain rotational dynamics in qualitative ways. Clues to the origin of grain alignment are presumably also contained in other phenomena discovered via molecular cloud

polarimetry, such as the relationship between the polarization-to-extinction ratio, P/A, and the extinction in molecular clouds (Tamura et al. 1987) and the wavelength dependence of linear polarization both in the near-infrared continuum (Wilking et al. 1980, 1982; Martin & Whittet 1990) and in infrared grain spectral features (e.g., Aitken et al. 1985) to name just a few examples.

This is the first paper in a two-part series on paramagnetic and super-paramagnetic grain alignment in the absence of suprathermal rotation— a scenario which we will refer to as "thermal alignment" for brevity. Our objective is to provide calculations which can be used to test this scenario, by comparing quantitative predictions with observations such as polarimetry of quiescent globules. In this paper we describe our numerical solution techniques (§2), discuss relevant physical processes in molecular clouds (§3), and describe some benchmark calculations which calibrate the accuracy of our calculations (§4). Our results are summarized in §5. In the second paper of this series (DeGraff, Roberge, & Flaherty 1993, hereafter Paper II), we present an exhaustive exploration of the parameter space for thermal alignment and describe an unambiguous observational test.

2 THE LANGEVIN EQUATION FOR BROWNIAN ROTATION

In this section we introduce the Langevin equation as an alternative to the Fokker-Planck equation for calculations on grain alignment. For a more thorough description of the Langevin equation and its equivalence to the Fokker-Planck equation, the reader is referred to the excellent monographs by Chandrasekhar (1943) and Gardiner (1990). For discussions of numerical solution techniques, see Fox (1987), Gard (1988), and references therein.

2.1 Equivalence of the Fokker-Planck and Langevin Equations

The Rayleigh reduction factor is a statistic of the distribution function, $f(\boldsymbol{J},t)$, for the grain rotational angular momenta at time t. In principle f can be found accurately by solving the Fokker-Planck (henceforth FP) equation,

$$\frac{\partial f}{\partial t}+\frac{\partial}{\partial J_i}\left(\langle \Delta J_i\rangle f\right)=\frac{1}{2}\frac{\partial^2}{\partial J_i \partial J_j}\left(\langle \Delta J_i\,\Delta J_j\rangle f\right), \quad i=x,y,z \tag{2.1}$$

(JS67; Cugnon 1971), where sums are implied by repeated subscripts, J_i is the i-th cartesian component of $\boldsymbol{J}$, and the mean torque,

$$\langle \Delta J_i \rangle \equiv \left\langle \frac{\Delta J_i}{\Delta t} \right\rangle, \quad i = x, y, z, \tag{2.2}$$

and "diffusion tensor,"

$$\langle \Delta J_i \, \Delta J_j \rangle \equiv \left\langle \frac{\Delta J_i \Delta J_j}{\Delta t} \right\rangle, \quad i, j = x, y, z, \tag{2.3}$$

are functions of $\boldsymbol{J}$ and t that can be found by evaluating the time averages denoted by angle brackets (see §3). The random variable $\Delta \boldsymbol{J}$ is the incremental change in $\boldsymbol{J}$ which is caused by the total external torque during the time interval Δt. Following common practice, we refer to the mean torque and diffusion tensor collectively as the "diffusion coefficients."

Solving the FP equation directly is a formidable problem (JS67; Cugnon 1971, 1983, 1985) because R is extremely sensitive to numerical errors in the calculated distribution function when the alignment is weak. For example, the linear polarization $P \sim 1\%$ which has been detected in the far-infrared and submillimeter emission from grains is consistent with $R \lesssim 0.1$ in some regions (Dragovan 1986). Now suppose that we wish to calculate $R = 0.1$ with modest accuracy, say 10%. Then it follows from eq. (1.1) that we must compute $\langle \cos^2 \beta \rangle$ with an accuracy $\sim 1\%$. Solving the FP equation for $f(\boldsymbol{J}, t)$ by finite difference methods would obviously require a large number of grid points in angular momentum space to satisfy even this modest accuracy requirement. It seems likely that perturbation methods could be developed to handle the weak alignment limit, but then one would still need to perform a finite difference calculation to find R when the grains are strongly aligned, a case which is also of practical interest (Lee & Draine 1985). Monte Carlo simulations present a viable method for calculating R (Purcell 1969; PS71), but are much less efficient than the techniques described below.

In this paper we describe a computational approach which works whether the alignment is strong or weak, yields R values accurate to typically $\sim 1\%$ with modest amounts of computation, and is no more difficult to implement than a Runge-Kutta algorithm for integrating an ordinary differential equation. Our method relies upon the well-known mathematical

equivalence of the FP equation and the "Langevin equation,"

$$dJ_i = A_i(\boldsymbol{J}, t)\, dt + B_{ij}(\boldsymbol{J}, t)\, dw_j, \quad i = x, y, z, \tag{2.4}$$

which is a stochastic differential equation for the random variable $\boldsymbol{J}(t)$. Here the angular impulse which is imparted to the grain during an infinitesimal time interval dt has been written as the sum of its mean value plus a fluctuating part corresponding, respectively, to the first and second terms on the right-hand side of eq. (2.4). As discussed below, a simple quadrature scheme can be used to integrate eq. (2.4) numerically as an initial value problem, yielding a pseudo-random, time-dependent variable, $\tilde{\boldsymbol{J}}(t)$, whose statistics converge to those of $\boldsymbol{J}(t)$ as discussed below. Moreover, it can be shown (e.g., Gardiner 1990) that the Langevin and FP equations describe the *same* random variable if one chooses $\boldsymbol{A}$ to be the mean torque,

$$A_i \equiv \langle \Delta J_i \rangle, \quad i = x, y, z, \tag{2.5}$$

and B to be the matrix square root of the diffusion tensor,

$$\left(BB^T\right)_{ij} \equiv \langle \Delta J_i\, \Delta J_j \rangle, \quad i, j = x, y, z, \tag{2.6}$$

where B^T is the transpose of B.

The statistical fluctuations in $d\boldsymbol{J}$ are characterized by the random functions dw_j in eq. (2.4). The requirement that $\boldsymbol{J}(t)$ should satisfy the FP equation uniquely determines $\{dw_j\}$ to be a vector of statistically independent "differential Wiener increments," which are defined as follows. The Wiener process is a random variable, $w(t)$, whose distribution function satisfies the one-dimensional FP equation

$$\frac{\partial f_w}{\partial t} = \frac{1}{2}\frac{\partial^2 f_w}{\partial w^2}, \tag{2.7}$$

i.e., the diffusion equation. The finite Wiener increment is defined to be the change in w,

$$\Delta w \equiv w(t_0 + \Delta t) - w(t_0), \tag{2.8}$$

where t_0 is some specified initial time, $w(t_0)$ is assumed to be known with certainty, and $\Delta t \equiv t - t_0$ is an arbitrary but finite time interval. One may verify by direct substitution into

the one-dimensional FP equation that the Wiener increments have a Gaussian distribution,

$$f_{\Delta w}(\Delta w) = (2\pi\,\Delta t)^{-1/2}\ \exp\left[-\left(\Delta w\right)^2/2\,\Delta t\right], \tag{2.9}$$

with zero mean,

$$\langle \Delta w \rangle = 0, \tag{2.10}$$

and variance,

$$\left\langle (\Delta w)^2 \right\rangle = \Delta t, \tag{2.11}$$

a familiar result from the theory of random walks. The infinitesimal Wiener increment is simply the limit of Δw as $\Delta t \longrightarrow dt$.

2.2 Numerical Integration Techniques

Suppose that we wish to solve the Langevin equation for the components of $\boldsymbol{J}(t)$ on some time interval, $[0, T]$, subject to the initial conditions

$$J_i(0) = J_{i,0}, \quad i = x, y, z, \tag{2.12}$$

where $\{J_{i,0}\}$ may be known with certainty or may themselves be random variables. We partition the interval $[0, T]$ into the uniform grid $t_n = n\Delta t,\ n = 0, \ldots, N$, where N is an integer and $\Delta t = T/N$. In the simplest numerical method for integrating eq. (2.4), called the Euler-Maruyama scheme, we set $J_i(t_n) \approx \tilde{J}_{i,n}$, where

$$\tilde{J}_{i,0} = J_{i,0}, \quad i = x, y, z \tag{2.13}$$

and

$$\tilde{J}_{i,n+1} = \tilde{J}_{i,n} + A_i\left(\tilde{\boldsymbol{J}}(t_n), t_n\right)\,\Delta t + B_{ij}\left(\tilde{\boldsymbol{J}}(t_n), t_n\right)\,\Delta w_j, \quad i = x, y, z \tag{2.14}$$

(Gard 1988). The starting values are obtained by sampling from the appropriate distribution if the initial conditions are random and the Wiener increments are obtained by sampling from the distribution given in eq. (2.9). Thus, the Euler-Maruyama scheme is a straightforward generalization of Euler's method for integrating nonrandom differential equations. The analogous Runge-Kutta schemes of higher order also exist, but they can be used only if the

diffusion tensor satisfies an additional symmetry condition and are not considered further here.

Each pseudo-random variable $\tilde{J}_i(t)$ is a numerical simulation of the time-dependent "sample path" followed by $J_i(t)$ as it traverses angular momentum space. If the diffusion coefficients satisfy certain smoothness and growth conditions, then $\tilde{J}_i(t)$ converges to $J_i(t)$ in the mean square square sense,

$$\lim_{\Delta t \to 0} \left\langle \left[\tilde{J}_i(t) - J_i(t) \right]^2 \right\rangle = 0 \tag{2.15}$$

(Gard 1988), where the angle brackets in eq. (2.15) denote expectation values at fixed t for a sequence of identical trial calculations, not time averages. The numerical solutions converge with the step size, Δt, at a rate such that the mean square error in $\tilde{J}_{i,n}$ is

$$\left\langle \left[\tilde{J}_{i,n} - J_i(t_n) \right]^2 \right\rangle = \mathcal{O}(\Delta t^m) \tag{2.16}$$

where $m = 2$ for a single step (local error) and $m = 1$ for N steps (global error). The smoothness and growth conditions cited above are mild (Gard 1988) and are satisfied for all problems discussed in this and subsequent papers in this series (Paper II; Roberge & Hanany 1993).

For reasons discussed below (§4), we are interested only in the steady state angular momentum distribution. Thus we compute the Rayleigh reduction factor from the sequence $\left\{ \tilde{J}_{i,n},\ n = 0, \ldots, N \right\}$ in the obvious way, by evaluating $\cos^2 \beta$ from the instantaneous value of the vectorial angular momentum at each time step and then taking the ensemble average, $\langle \cos^2 \beta \rangle$, to be the time average of $\cos^2 \beta$ over a long sequence of consecutive steps. The time averaging begins at a time which is sufficiently large so that the grain has "forgotten" its initial conditions, which are therefore arbitrary. The total averaging time, T, is determined by the requirement that statistical fluctuations in the running average of $\langle \cos^2 \beta \rangle$ should be sufficiently small to guarantee the convergence of R to within a predefined tolerance. The exact value of T and other details of our calculations are described in §4.

Integrating the Langevin equation is similar to the Monte Carlo method in that both methods simulate the sample paths of $\boldsymbol{J}(t)$ and that the root-mean-square error in $\langle \cos^2 \beta \rangle$

is inversely proportional to the square root of the total integration or simulation time.[1]

[1] This assertion is justified in §4 for the Langevin equation method.

However, the Langevin equation has several significant advantages over the Monte Carlo technique. First, a computer code to integrate eq. (2.4) requires just a few lines of code to perform the time step in eq. (2.14) plus instructions to evaluate $\boldsymbol{A}$, B, the Wiener increments, and the running average of $\cos^2\beta$. In contrast, the Monte Carlo method requires direct simulations of all relevant physical processes, each of which may require several steps. For example, simulating a gas-grain collision involves choosing the arrival time, thermal velocity, and collision site of the incident gas particle from the appropriate distributions and then simulating the stochastic dynamics of the collision. Second, the convergence theorems above guarantee that statistics such as R which are calculated numerically via the Langevin equation converge to the statistics of the exact distribution, f, and provide guidance for estimating the dependence of statistical errors on Δt and T. Finally, integrating the Langevin equation eliminates "coarse graining" procedures which are unavoidable in the Monte Carlo method. For example, the number of gas-grain collisions (typically $\sim 10^9$ during each correlation time of the random motion of a real grain) must be reduced to a manageable number by arbitrarily scaling up the masses of the gas particles in a Monte Carlo simulation. The only assumptions incorporated in the Langevin equation are those on which the FP equation itself is based— that $\boldsymbol{J}(t)$ is a Markovian random variable and has continuous sample paths.

3 DIFFUSION COEFFICIENTS FOR THERMAL GRAIN ALIGNMENT

In this section we calculate the diffusion coefficients for various physical processes on the *ad hoc* assumption that the grain rotational energies are of order kT_g, where T_g is the gas kinetic temperature. Analogous calculations for the alternative, suprathermal alignment scenario (P79) will be presented in a future paper.

3.1 Assumptions

3.1.1 Grain Properties

We adopt a two-component model in which each grain consists of a refractory core surrounded by a volatile ice mantle, both of which are at a common temperature, T_d. Because the grain composition is controversial, we give analytic expressions for the diffusion coefficients wherein arbitrary grain models can be represented by appropriate choices of various material properties. Thus in the present paper we treat the i-th grain component (where $i = c$ or m) as an unspecified, homogeneous solid with mass density ρ_i, complex magnetic susceptibility $\chi_i = \chi_i' + i\chi_i''$, and complex dielectric function $\epsilon^{(i)}(\lambda)$ at wavelength λ. We assume that the imaginary component of χ_i is given by an expression of the form

$$\chi_i'' = K_i \Omega \tag{3.1}$$

(JS67), where Ω is the grain angular velocity and the quantity K_i sets the time scale for alignment by paramagnetic or super-paramagnetic torques (cf. §3.7). For a broad range of ordinary paramagnetic materials,

$$K_i \approx \frac{2.5 \times 10^{-12} \text{ Kelvin-s}}{T_d} \tag{3.2}$$

(Purcell 1969; Spitzer 1978). For super-paramagnetic grains, K_i is larger by an uncertain factor $\lesssim 10^3$–10^5 (JS67; Duley 1978) and the real part of χ_i is similarly enhanced over typical values for ordinary substances. We assume that the principle of superposition holds for the volume susceptibility, so that

$$K = \frac{V_c K_c + V_m K_m}{V} \tag{3.3}$$

is the effective K-value for the grain as a whole, where V_c and V_m are the core and mantle volumes, respectively, and $V \equiv V_c + V_m$ is the total grain volume.

The shapes of interstellar grains are constrained by models of the wavelength-dependence of extinction and polarization in the vicinity of grain spectral features (Lee & Draine 1985; Draine 1988). The limited observational evidence which is presently available on molecular cloud grains (Aitken et al. 1985; Lee & Draine 1985; Hildebrand 1988b) suggests that they

are "typically" oblate, with modest axis ratios $\sim$ 2:1. In this paper we model the grains as oblate spheroids, there being no apparent reason for considering ellipsoids or other more complicated shapes.[2] Following the notation of Draine & Lee (1984), we take the mantle surface to be a spheroid with semiaxes a_m parallel to the symmetry axis and $b_m > a_m$ perpendicular to the symmetry axis. We assume for simplicity that the core-mantle interface is a spheroid confocal with the mantle surface and denote the core semi-axes by a_c and b_c. The eccentricity of the i-th component,

$$e_i \equiv \sqrt{1-(a_i/b_i)^2}, \tag{3.4}$$

may be different for $i = c$ and $i = m$. The mass of our model grain is

$$M_d = \frac{4}{3}\pi b_m^2 a_m \rho_m \left\{1 + \left(\frac{\rho_c}{\rho_m} - 1\right)\left(\frac{b_c}{b_m}\right)^2\left(\frac{a_c}{a_m}\right)\right\} \tag{3.5}$$

and its inertia tensor has components

$$I_{zz}^b = \frac{8\pi}{15}\rho_m a_m b_m^4 \Theta_{zz} \tag{3.6}$$

for rotation about the symmetry axis and

$$I_{xx}^b = \frac{4\pi}{15}\rho_m a_m b_m^4 \left(1 + a_m^2/b_m^2\right)\Theta_{xx} \tag{3.7}$$

for rotation about any axis perpendicular to the symmetry axis, where the factors

$$\Theta_{zz} \equiv 1 + \left(\frac{\rho_c}{\rho_m} - 1\right)\left(\frac{a_c}{a_m}\right)\left(\frac{b_c}{b_m}\right)^4 \tag{3.8}$$

and

$$\Theta_{xx} \equiv 1 + \left(\frac{\rho_c}{\rho_m} - 1\right)\left(\frac{a_c}{a_m}\right)\left(\frac{b_c}{b_m}\right)^4 \frac{(1 + a_c^2/b_c^2)}{(1 + a_m^2/b_m^2)} \tag{3.9}$$

vary from unity for homogeneous grains to ρ_c/ρ_m for bare grains with no ice mantles.

[2] That is, one can model observations of interstellar polarization successfully without resorting to more complicated shapes (Hildebrand 1988b). However the grain shape might have a dramatic effect on the dynamics of alignment. For example, Mathis (private communication) has noted that suprathermal rotation might be driven by gas-grain collisions and evaporation from the large-scale surface structures on a highly irregular grain. Consideration of this interesting possibility is deferred to a future paper on suprathermal spinup processes in molecular clouds.

3.1.2 Gas Properties

Our model grains are assumed to be located in a cloud which has a constant, uniform number density, n, and magnetic field, $\boldsymbol{B}$, and which is composed entirely of H_2 molecules with mass m. The gas particles are assumed to have a Maxwellian velocity distribution with kinetic temperature T_g in a reference frame (the "gas frame") where the bulk velocity of the gas is zero. We solve the Langevin equation for the components of $\boldsymbol{J}$ in the gas frame under the assumption that the latter is an *inertial* reference frame; however, our calculations should also be accurate for accelerating plasmas whenever the time scale for acceleration is much longer than the time to establish the steady state angular momentum distribution. The latter is strictly less than the "gas damping time," t_{gas} (cf. eq. [3.31]), which in turn is comparable to the time it takes a grain to collide with an amount of gas equal to its own mass. Numerical estimates of t_{gas} and some other relevant time scales are given in Table 1. The center of mass (CM) velocity of the grain in the gas frame is assumed to satisfy $v_d \ll v_{th}$, where the gas thermal speed is defined to be

$$v_{th} \equiv \left(\frac{2kT_g}{m}\right)^{1/2} . \tag{3.10}$$

Radiation pressure and other forces can cause a grain to drift through the gas at speeds $v_d \geq v_{th}$ in some environments, with significant consequences for the alignment process (Gold 1952; Purcell 1969; PS71). These effects will be studied in detail in a subsequent paper (Roberge & Hanany 1993) but are not considered here.

3.2 Frames of Reference

We solve the Langevin equation in the gas frame but in some cases it is easier to calculate the diffusion coefficients in a "body frame" whose axes are aligned instantaneously with the grain's principal axes of inertia. Henceforth, vector and tensor components without superscripts will refer to the gas frame, whose cartesian basis vectors, $(\hat{x}, \hat{y}, \hat{z})$, have $\hat{z}$ oriented along the magnetic field and $\hat{x}$ and $\hat{y}$ oriented arbitrarily in the plane normal to $\boldsymbol{B}$. Vector and tensor components with a superscript "b" will refer to the body frame, whose basis vectors, $\left(\hat{x}^b, \hat{y}^b, \hat{z}^b\right)$, have $\hat{z}^b$ oriented parallel to the grain symmetry axis and the axes $\hat{x}^b$ and

$\hat{y}^b$ oriented arbitrarily in the equatorial plane. Henceforth we will refer to $\hat{z}^b$ as the "major axis of inertia" because $I^b_{zz} > I^b_{xx}$. While the body frame axes are parallel to the principal axes of inertia, they are defined to be stationary in the gas frame and so *do not corotate with the grain material.* Thus the body frame is an inertial frame which is defined independently at each time by the instantaneous grain orientation.

We specify the relative orientation of the gas and body frames in terms of the familiar Eulerian angles (Fig. 1). In setting one of the Eulerian angles equal to β, we have anticipated the result (P79, §3.4) that $\boldsymbol{J}$ is closely aligned with the major axis of inertia at all times. The cartesian components of the mean torque and diffusion tensor transform according to

$$\langle \Delta J_i \rangle = G_{ij} \left\langle \Delta J^b_j \right\rangle \tag{3.11}$$

and

$$\langle \Delta J_i \, \Delta J_j \rangle = G_{im} \left\langle \Delta J^b_m \, \Delta J^b_n \right\rangle G^{-1}_{nj}. \tag{3.12}$$

where the transformation matrix is given in terms of the Eulerian angles by

$$G = C \, D \, E \tag{3.13}$$

with

$$C = \begin{pmatrix} \cos\phi & -\sin\phi & 0 \\ \sin\phi & \cos\phi & 0 \\ 0 & 0 & 1 \end{pmatrix}, \tag{3.14}$$

$$D = \begin{pmatrix} 1 & 0 & 0 \\ 0 & \cos\beta & -\sin\beta \\ 0 & \sin\beta & \cos\beta \end{pmatrix}, \tag{3.15}$$

and

$$E = \begin{pmatrix} \cos\psi & -\sin\psi & 0 \\ \sin\psi & \cos\psi & 0 \\ 0 & 0 & 1 \end{pmatrix} \tag{3.16}$$

(Goldstein 1950).

3.3 Fluctuation-Dissipation Theorem

There is a useful relationship between the diffusion coefficients for any physical process which tends, in the absence of other processes, to establish thermal equilibrium (e.g., Reichl 1980). In particular, the mean torque about the major axis of inertia is given by

$$\left\langle \Delta J_z^b \right\rangle \;=\; -J_z^b / t_{damp} \tag{3.17}$$

(cf. P79, eq. [1]), where the damping time,

$$t_{damp} = \frac{2 I_{zz}^b kT}{\left\langle (\Delta J_z^b)^2 \right\rangle}, \tag{3.18}$$

depends on the diffusion tensor and the temperature, T, at which thermal equilibrium prevails. Analogous relations exist for rotation about the other principal axes, but are not relevant here for reasons discussed below. Of course the alignment of interstellar grains is inherently a nonequilibrium situation, due to the different temperatures which are generally associated with different processes. Nevertheless, one can use the Fluctuation-Dissipation Theorem to find the mean torque for any individual process, such as thermal emission (see §3.8.3), which is characterized by a unique temperature.

3.4 Internal Dissipation of Rotational Energy

This term refers collectively to processes first described by Purcell (P79) which align the major axis of inertia with $\boldsymbol{J}$. According to Purcell's analysis, the most efficient of these processes is associated with the Barnett effect, in which the transfer of angular momentum from bulk rotation to aligned spins or orbits produces a magnetization

$$\boldsymbol{M} = \chi \, \boldsymbol{\Omega} / \gamma \tag{3.19}$$

in a grain rotating with angular velocity $\boldsymbol{\Omega}$. Here γ is the magnetogyric ratio of the aligned magnetic moments. Purcell observed that the magnetization in eq. (3.19) is identical to that which would be produced by applying a "Barnett equivalent" magnetizing field $\boldsymbol{H}_{Be} = \boldsymbol{\Omega}/\gamma$ and, further, that if $\boldsymbol{J}$ is not aligned along a principal axis of the grain then $\boldsymbol{\Omega}$, and hence the effective applied field, are nonsteady in a reference frame fixed to the grain. Magnetization

of the grain material by such a nonsteady "field" leads to paramagnetic absorption and the dissipation of rotational energy as in the Davis-Greenstein mechanism, except that the roles which are played in the DG mechanism by $\boldsymbol{B}$ and $\boldsymbol{J}$ are played in Barnett relaxation by $\boldsymbol{\Omega}$ and the major axis of inertia, respectively. Further, because Barnett relaxation involves no external torques, $\boldsymbol{J}$ is a conserved quantity.[3] The transformation of rotational kinetic energy into heat by Barnett relaxation drives the grain toward the state of smallest rotational energy consistent with a given value of $\boldsymbol{J}$, i.e., toward rotation about the major axis of inertia (P79).

[3] This statement is not strictly true. The quantity which is conserved is obviously the total grain internal angular momentum, $\boldsymbol{F}$, which includes not only rotation but also the angular momentum $\boldsymbol{S}$ associated with the magnetization. However, for a homogeneous, oblate spheroid with equatorial radius b_m composed of a paramagnetic or super-paramagnetic substance with partially aligned electron spins, one can show that

$$S/J = 5\chi'_m m_e^2 c^2/2e^2\rho_m b_m^2 \approx 10^{-4}\chi'_m \rho_{m,0}^{-1} b_{m,-5}^{-2},$$

where e and m_e are respectively the electron charge and mass and the notation $\rho_{m,0}$ means $\rho_m/10^0$ g cm^{-3} and similarly for the values of other quantities in Gaussian cgs units. Thus, even for super-paramagnetic grains, the ratio of spin-to-rotational angular momentum is only $S/J \lesssim 1\%$. We will therefore ignore the distinction between $\boldsymbol{J}$ and $\boldsymbol{F}$, an assumption which is also implicit in Purcell's (P79) discussion of Barnett relaxation.

For interstellar grains, the time scale, t_{bar}, for Barnett relaxation is always many orders of magnitude longer than the grain rotational period (Table 1). For spheroidal grains the motion of $\boldsymbol{\Omega}$ in grain coordinates is therefore essentially that of a free symmetric top over times small compared to t_{bar}. From this information one can easily compute the energy dissipation rate and from it the rate of change of the angle θ between $\boldsymbol{\Omega}$ and the major axis of inertia. Applying Purcell's analysis to the case of an oblate, spheroidal, core-mantle grain, we find that

$$\frac{d\theta}{dt} = -\frac{VKh^2(h-1)J^2}{\gamma^2(I_{zz}^b)^3}\sin\theta\cos\theta, \tag{3.20}$$

where K is defined in eq. (3.3), V is the total grain volume, and

$$h \equiv I_{zz}^b/I_{xx}^b. \tag{3.21}$$

We will define the Barnett alignment time to be

$$t_{bar} \equiv \left| \frac{\theta}{\dot{\theta}} \right|_{\theta=\pi/4} . \tag{3.22}$$

A numerical estimate for molecular cloud grains is given in Table 1. As Purcell pointed out, t_{bar} is typically so short in comparison to the time scales for $\boldsymbol{J}$ to be changed by collisional or magnetic torques, that one may consider the axis of largest rotational inertia to be aligned with $\boldsymbol{J}$ at all times. This conclusion is reinforced if one includes the other dissipative mechanism discussed by Purcell, rotational anelasticity, although the latter is typically one to two orders of magnitude less efficient than Barnett relaxation (P79). We note that this is the *only* consequence of internal dissipation on the alignment processes considered here because, as discussed in the footnote above, Barnett relaxation and rotational anelasticity conserve $\boldsymbol{J}$ to an excellent degree.

3.5 Larmor Precession

Barnett magnetization endows a spheroid rotating about its major axis of inertia with a steady magnetic moment

$$\boldsymbol{\mu}_{bar} = \frac{\chi' V}{\gamma I_{zz}^b} \boldsymbol{J}, \tag{3.23}$$

where $\chi' \equiv (V_c \chi_c' + V_m \chi_m')/V$. The magnetic torque $\boldsymbol{\mu}_{bar} \times \boldsymbol{B}$ causes $\boldsymbol{J}$ to precess about $\boldsymbol{B}$ at the Larmor frequency, $\Omega_{lar} = 2\pi/t_{lar}$, where the Larmor period is

$$t_{lar} = \frac{2\pi\gamma I_{zz}^b}{\chi' V B}. \tag{3.24}$$

There is also a relatively small contribution to the magnetic moment from rotating surface charges. For an oblate spheroid with charge Q uniformly distributed over its surface, the neglected magnetic moment would be smaller than the Barnett moment by a factor

$$\frac{\mu_{chg}}{\mu_{bar}} = \frac{3\,Q\,\gamma\,X}{8\,\pi\,c\chi'\,(a_m/b_m)\,b_m}\,, \tag{3.25}$$

where X is a numerical factor which varies from 2/3 for spheres to 1/2 for thin disks. The ratio (3.25) is typically only $\mathcal{O}(10^{-5})$ and we will neglect μ_{chg}. Representative values of the Larmor period are given in Table 1.

The Larmor period is always several orders of magnitude shorter than the time scales for $\boldsymbol{J}$ to be changed by the collisional, paramagnetic, and radiative torques discussed below. It is therefore appropriate to average the diffusion coefficients for these torques over a uniform distribution of the Larmor precession angle, ϕ, in Fig. 1. This is the only effect of Larmor precession on our calculations: once the diffusion coefficients for the other torques have been Larmor-averaged, it becomes unnecessary to include the torque $\boldsymbol{\mu}_{bar}\times\boldsymbol{B}$ explicitly in the Langevin equation. (Note that Larmor precession has no effect on internal dissipation, even though the Larmor period can be shorter than the Barnett alignment time scale. This is because rotation about the axis of largest rotational inertia is the state of minimum kinetic energy for a given value of J and the Larmor torque is conservative.)

For each of the processes considered below, the diffusion tensor is diagonal in the body frame with cartesian components

$$\left\langle \Delta J_i^b \, \Delta J_j^b \right\rangle = \begin{pmatrix} \left\langle (\Delta J_\perp^b)^2 \right\rangle & 0 & 0 \\ 0 & \left\langle (\Delta J_\perp^b)^2 \right\rangle & 0 \\ 0 & 0 & \left\langle (\Delta J_\parallel^b)^2 \right\rangle \end{pmatrix}, \tag{3.26}$$

where the subscripts "$\parallel$" and "$\perp$," respectively, denote body frame axes which are parallel and normal to the symmetry axis. Transforming these components to the gas frame using eq. (3.12) and averaging over the phase angles ϕ for Larmor precession and ψ for rotation, we find the diffusion tensor in the gas frame. The latter is also diagonal with components

$$\left\langle (\Delta J_x)^2 \right\rangle = \frac{1}{2}\left\{ (1+\cos^2\beta)\left\langle (\Delta J_\perp^b)^2 \right\rangle + \sin^2\beta \left\langle (\Delta J_\parallel^b)^2 \right\rangle \right\}, \tag{3.27}$$

$$\left\langle (\Delta J_y)^2 \right\rangle = \left\langle (\Delta J_x)^2 \right\rangle, \tag{3.28}$$

and

$$\left\langle (\Delta J_z)^2 \right\rangle = \sin^2\beta \left\langle (\Delta J_\perp^b)^2 \right\rangle + \cos^2\beta \left\langle (\Delta J_\parallel^b)^2 \right\rangle. \tag{3.29}$$

3.6 Gas-Grain Collisions and Thermal Evaporation

The diffusion coefficients for gas-grain collisions and thermal evaporation have been calculated in Appendixes A–C under the following assumptions: (1) We assume that every

colliding H_2 molecule sticks to the surface long enough (i.e., a few times the surface oscillation period for physisorbed H_2) so that its kinetic energy becomes thermalized at the grain temperature; (2) we assume that every sticking collision is followed by thermal evaporation and that the velocity distribution of evaporating molecules is determined by the principle of detailed balancing (Burke & Hollenbach 1983); (3) we assume that evaporation occurs uniformly over the grain surface, i.e., that there are no preferred evaporation sites; and (4) we set the gas-grain drift velocity to $\boldsymbol{v}_d = 0$ as discussed above. Assumptions (1)–(2) should be excellent approximations for H_2 colliding at thermal energies either with cold grains (with $3 < T_d \lesssim 15$ K) covered with H_2 or with warmer grains whose ice mantles are devoid of H_2 (see the discussion in Tielens & Allamandola 1987). Assumption (3) is consistent with the thermal alignment hypothesis under consideration in this paper, but might be inappropriate for real grains if the latter are highly irregular (see the footnote in §3.1.1). Nevertheless, item (3) is plausible because any preferred evaporation sites, if present, will generally have lifetimes that are smaller than the time to establish suprathermal rotation (which is comparable to t_{gas}). For example, thermal diffusion of the H_2 molecules on a cold grain will rearrange the surface topography on a time scale, $t \ll 1$ s, which is always negligible compared to t_{gas}. For warmer grains, the corresponding time scale for H_2O diffusion on an H_2O surface is still less than t_{gas} if $T_d \gtrsim 30$ K. See Tielens & Allamandola (1987) and references therein.

Within the above approximations, the the mean torque for collisions plus evaporation has gas frame components

$$\langle \Delta J_i \rangle_{c+ev} = -J_i / t_{gas} \tag{3.30}$$

where

$$t_{gas} \equiv \frac{3}{4\sqrt{\pi}} \frac{I_{zz}^b}{n m v_{th} b_m^4 \Gamma_{\|}(e_m)} \tag{3.31}$$

is the gas damping time. The diffusion tensor is diagonal in the body-frame with components

$$\left\langle (\Delta J_{\|}^b)^2 \right\rangle_{c+ev} = \frac{2\sqrt{\pi}}{3} n m^2 b_m^4 v_{th}^3 \left(1 + \frac{T_d}{T_g}\right) \Gamma_{\|}(e_m) \tag{3.32}$$

and

$$\left\langle (\Delta J_{\perp}^b)^2 \right\rangle_{c+ev} = \frac{2\sqrt{\pi}}{3} n m^2 b_m^4 v_{th}^3 \left(1 + \frac{T_d}{T_g}\right) \Gamma_{\perp}(e_m). \tag{3.33}$$

The only mathematical approximation used in deriving expressions (3.30)–(3.33) is the neglect of terms of order $\sqrt{m/M_d}$ and higher (Appendix C). The grain shape enters only via the "eccentricity factors,"

$$\Gamma_{\|}(e_m) = \frac{3}{16}\left\{ 3 + 4(1-e_m^2)g(e_m) - e_m^{-2}\left[1-(1-e_m^2)^2 g(e_m)\right]\right\} \tag{3.34}$$

and

$$\Gamma_{\perp}(e_m) = \frac{3}{32}\left\{ 7 - e_m^2 + (1-e_m^4)g(e_m) + (1-2e_m^2)\left[1+e_m^{-2}\left[1-(1-e_m^2)^2 g(e_m)\right]\right]\right\}, \tag{3.35}$$

where

$$g(e_m) \equiv \frac{1}{2e_m}\ln\left(\frac{1+e_m}{1-e_m}\right) \tag{3.36}$$

and e_m is the eccentricity of the mantle surface. These functions have the limiting values

$$\lim_{e_m\to 0}\Gamma_{\|}(e_m) = \lim_{e_m\to 0}\Gamma_{\perp}(e_m) = 1 \tag{3.37}$$

for spheres and

$$\lim_{e_m\to 1}\Gamma_{\|}(e_m) = \lim_{e_m\to 1}\Gamma_{\perp}(e_m) = \frac{3}{8} \tag{3.38}$$

for infinitely thin disks. The eccentricity factors are plotted in Fig. 2. One can easily verify that the diffusion coefficients in eq. (3.30)–(3.33) satisfy the Fluctuation-Dissipation Theorem and reduce to the expressions derived by Jones & Spitzer (JS67) for spheres in the appropriate limit.

We obtain the gas frame components of the diffusion tensor by substituting eq. (3.32)–(3.33) into eq. (3.27)–(3.29) with the result that

$$\left\langle(\Delta J_x)^2\right\rangle_{c+ev} = \frac{\sqrt{\pi}}{3}nm^2b_m^4v_{th}^3\left(1+\frac{T_d}{T_g}\right)\left[\left(1+\cos^2\beta\right)\Gamma_{\perp} + \sin^2\beta\,\Gamma_{\|}\right], \tag{3.39}$$

$$\left\langle(\Delta J_y)^2\right\rangle_{c+ev} = \left\langle(\Delta J_x)^2\right\rangle_{c+ev}, \tag{3.40}$$

and

$$\left\langle(\Delta J_z)^2\right\rangle_{c+ev} = \frac{2\sqrt{\pi}}{3}nm^2b_m^4v_{th}^3\left(1+\frac{T_d}{T_g}\right)\left[\sin^2\beta\,\Gamma_{\perp} + \cos^2\beta\,\Gamma_{\|}\right]. \tag{3.41}$$

3.7 Paramagnetic or Super-Paramagnetic Absorption

Jones & Spitzer (JS67) derived the diffusion coefficients for paramagnetic or super-paramagnetic absorption in a spheroidal grain. The mean torque has gas frame components

$$\langle \Delta J_i \rangle_{mag} = -J_i / t_{mag}, \quad i = x, y, \tag{3.42}$$

and

$$\langle \Delta J_z \rangle_{mag} = 0. \tag{3.43}$$

The magnetic damping time for a core-mantle grain is

$$t_{mag} \equiv \frac{I_{zz}^b}{KVB^2}. \tag{3.44}$$

The diffusion tensor is diagonal with gas frame components

$$\left\langle (\Delta J_i)^2 \right\rangle_{mag} = 2kT_d VB^2 K, \quad i = x, y, \tag{3.45}$$

and

$$\left\langle (\Delta J_z)^2 \right\rangle_{mag} = 0. \tag{3.46}$$

These diffusion coefficients satisfy the Fluctuation-Dissipation Theorem by construction.

3.8 Electric Dipole Emission and Absorption

The angular momentum of a grain is changed by the emission, absorption, and scattering of photons. Purcell & Spitzer (PS71) pointed out that radiative processes generally contribute to both the mean torque and diffusion tensor and estimated the diffusion coefficients for spherical grains in equilibrium with a thermal radiation bath at temperature $T_{rad} = T_d$. In view of the growing body of observations on polarized thermal emission from dust, especially the warm dust with $T_d \sim 100$ K near the Galactic center (Werner et al. 1988; Hildebrand et al. 1990, 1992), it is appropriate to give a quantitative description of these effects for nonspherical grains. We therefore calculate the diffusion coefficients for emission from and absorption by oblate, spheroidal, core-mantle grains and consider explicitly the nonequilibrium case where $T_{rad} \neq T_d$. The only assumption used in the following discussion

is that the grain-photon interaction is in the Rayleigh limit. This is a good approximation for bare silicate grains with radii $b_c \leq 1$ μm and graphite grains with radii $b_c \leq 0.1$ μm if the photon wavelengths are $\lambda \gtrsim 10$ μm (Draine & Lee 1984). The following discussion therefore applies mainly to grains that are shielded from direct sources of optical and UV photons. Grain alignment and disalignment by short-wavelength radiation (Harwit 1970), which might be important in photodissociation regions, is not considered here.

3.8.1 Electric Dipole Cross Section of a Rotating Dielectric Spheroid

In the electric dipole approximation, scattering is negligible and the grain absorption cross section at frequency ω is given by a simple analytic expression (van de Hulst 1981). The cross section for a *non-rotating* grain interacting with a linearly polarized plane wave whose electric field vector, $\boldsymbol{E}$, lies parallel to the j-th principal grain axis is

$$C_j(\omega) = \frac{4\pi\omega}{c} \, \mathrm{Im}\left(\alpha^e_{jj}\right) \quad j = \parallel, \perp, \tag{3.47}$$

where ω is the circular frequency of the wave and α^e_{jj} is the electric polarizability of the grain for $\boldsymbol{E}$ polarized along the j-th body frame axis. The polarizability tensor of a spheroidal core-mantle grain can be expressed in terms of the dielectric functions of the core and mantle materials, the grain eccentricity, and the core-to-mantle volume ratio. For details, see Draine & Lee (1984).

There is a small correction to expression (3.47) when the grain rotates, which arises because the dielectric polarization of the grain depends on the frequency of $\boldsymbol{E}$ relative to the grain material. Consider an oblate spheroid rotating about its symmetry axis with angular velocity $\Omega = J/I^b_{zz}$. Let E_0 be the electric field amplitude of an incident plane wave and let ζ be the angle between the electromagnetic wavevector, $\boldsymbol{k}$, and the grain rotation axis, $\hat{z}^b$. It is useful to take the two independent polarization states of the incident wave to be the states of positive and negative helicity, corresponding to left and right circular polarization, respectively. Define a set of rotating basis vectors, $(\hat{x}^r, \hat{y}^r, \hat{z}^r)$, which are fixed to the grain material with $\hat{z}^r$ along the rotation axis and with $\hat{x}^r$ and $\hat{y}^r$ oriented arbitrarily in the grain's equatorial plane. One can easily show by a suitable transformation of coordinates that the

electric field components in the rotating frame attached to the grain are

$$E_x^r(\pm) = \frac{1}{2}E_0\left\{\left[\cos\zeta \mp 1\right]\cos\left(\omega+\Omega\right)t \;+\; \left[\cos\zeta \pm 1\right]\cos\left(\omega-\Omega\right)t\right\}, \tag{3.48}$$

$$E_y^r(\pm) = -\frac{1}{2}E_0\left\{\left[\cos\zeta \mp 1\right]\sin\left(\omega+\Omega\right)t \;-\; \left[\cos\zeta \pm 1\right]\sin\left(\omega-\Omega\right)t\right\}, \tag{3.49}$$

and

$$E_z^r(\pm) = -E_0\,\sin\zeta\,\cos\omega t, \tag{3.50}$$

where the upper (lower) sign choice corresponds to the case where the incident wave has positive (negative) helicity. Thus in general the grain material "sees" three waves: a wave at the incident frequency, ω, which is linearly polarized along the grain rotation axis and two waves at frequencies $\omega \pm \Omega$ which are circularly polarized in the plane normal to the rotation axis. If we assume the grain material to be a linear dielectric, then the cross section for the sum of these waves is just the sum of the cross sections for the three frequency components weighted by their respective squared amplitudes. It folows that

$$C(\zeta,\pm) = \frac{1}{4}\left[\cos\zeta \mp 1\right]^2 C_\perp(\omega+\Omega) \;+\; \frac{1}{4}\left[\cos\zeta \pm 1\right]^2 C_\perp(\omega-\Omega) + \frac{1}{2}\sin^2\zeta\, C_\parallel(\omega), \tag{3.51}$$

is the electric dipole absorption cross section for a circularly polarized wave propagating at angle ζ with respect to the symmetry axis, where the upper and lower sign choices correspond to the positive and negative helicity states of the incident wave.

3.8.2 Absorption in an Isotropic Radiation Field

Expression (3.51) implies that a rotating grain absorbing photons from an isotropic radiation field will be slowed by rotational friction. The effect, which was first described by Purcell & Spitzer (PS71), is illustrated by the special case of a wave propagating parallel to the rotation axis ($\zeta = 0$). According to eq. (3.51), the absorption cross section for such a wave is $C(0,+) = C_\perp(\omega-\Omega)$ if the wave has positive helicity and $C(0,-) = C_\perp(\omega+\Omega)$ if it has negative helicity. Of course this is just what one expects in this special example: the incident wave has $\boldsymbol{E}$ circularly polarized in the equatorial plane of the grain with $\boldsymbol{E}$

rotating in the same (opposite) sense as the grain if the helicity is positive (negative). If the electric dipole cross section increases with frequency[4] then the grain is more likely to absorb the negative helicity wave. Recalling that in the electric dipole limit the photon orbital angular momentum is negligible compared to its spin angular momentum and that the spin of a positive (negative) helicity photon is parallel (antiparallel) to $\boldsymbol{k}$, we see that the cross section is larger for the absorption of photons which tend to decrease $\boldsymbol{J}$. This is the rotational friction noted above.

[4] At frequencies where this assumption is violated, the torque due to electric dipole absorption tends to spin up a rotating grain. Suprathermal spinup will occur if (a) $C_\perp$ decreases with ω over a sufficiently large fraction of the frequency range where photoabsorption is important and (b) the photoabsorption damping time is small compared to the damping time scales for other processes. However, neither (a) nor (b) is satisfied by the model silicate grains considered below.

Now consider the mean torque, $\langle \Delta \boldsymbol{J} \rangle_{abs}$, due to photoabsorption in an unpolarized, *isotropic* field. (The generalization to anisotropic radiation is obvious and will not be considered explicitly here.) The contribution to $\langle \Delta \boldsymbol{J} \rangle_{abs}$ from a pencil beam of photons with wavevectors in an infinitesimal solid angle dW centered about the unit vector $\hat{\boldsymbol{k}}$ and frequencies in the infinitesimal interval $d\omega$ centered about ω has body frame components

$$d\left\langle \Delta J_i^b \right\rangle_{abs} = \frac{\hbar}{2} I_\omega \left[C(\zeta,+) - C(\zeta,-) \right] \hat{k}_i^b \, dW \, d\omega \tag{3.52}$$

where I_ω is the monochromatic specific intensity of the radiation in photons $\mathrm{cm}^{-2}\ \mathrm{s}^{-1}\ \mathrm{sr}^{-1}$ s. The term in eq. (3.52) which depends on the grain cross sections can be expressed in terms of the electric dipole cross sections for linearly polarized light using eq. (3.51). The algebra is simplified if we note first that $\Omega \ll \omega$ in all cases of practical interest. For example, if we consider a homogeneous grain with rotational energy equal to the equipartition energy at the gas temperature and take a typical photon energy to be kT_{rad}, then

$$\frac{\Omega}{\omega} \sim 10^{-6}\, T_{g,1}^{1/2}\, \rho_{m,0}^{-1/2}\, b_{m,-5}^{-5/2} \left(1 - e_m^2\right)^{-1/4} T_{rad}^{-1}. \tag{3.53}$$

The ratio in eq. (3.53) wll therefore be much less than unity even if the grain rotates at a

highly suprathermal energy. Thus, to within an excellent approximation we may set

$$C_\perp(\omega \pm \Omega) \approx C_\perp(\omega) \pm C'_\perp \Omega \tag{3.54}$$

in expression (3.51), where

$$C'_\perp \equiv \frac{dC_\perp}{d\omega}. \tag{3.55}$$

Making use of approximation (3.54), we find that

$$C(\zeta,+) - C(\zeta,-) \;\approx\; -2\,\Omega\, C'_\perp \cos\zeta. \tag{3.56}$$

Substituting expression (3.56) into eq. (3.52), writing out the body frame components of $\hat{k}$ and performing the integrals over solid angle, we find that

$$\langle \Delta \boldsymbol{J} \rangle_{abs} = -\boldsymbol{J}/t_{abs}, \tag{3.57}$$

where the photoabsorption damping time is

$$t_{abs} = \frac{3I^b_{zz}}{4\pi\hbar} \left\{ \int_0^\infty C'_\perp I_\omega d\omega \right\}^{-1}. \tag{3.58}$$

In setting the upper limit of the frequency integral above to infinity, we are assuming the radiation temperature to be sufficiently small so that the integrand is only significant at frequencies where the electric dipole approximation is valid. For a thermal radiation field with temperature $T_{rad} \leq 100$ K, the fraction of photons with wavelengths $\lambda < 10$ μm is less than 10^{-4}.

The incremental contribution to the diffusion tensor from the monochromatic pencil beam discussed above has cartesian components

$$d\left\langle \Delta J^b_i \Delta J^b_j \right\rangle_{abs} = \frac{\hbar^2}{2} I_\omega \left[C(\zeta,+) + C(\zeta,-) \right] \hat{k}^b_i \hat{k}^b_j \, dW \, d\omega \tag{3.59}$$

in the body frame. Substituting expressions (3.51) for the cross sections into eq. (3.59), writing out the body frame components of $\hat{k}$, and performing the integral over solid angle, we find that the diffusion tensor is diagonal with nonzero components

$$\left\langle \left(\Delta J^b_\parallel\right)^2 \right\rangle_{abs} = \frac{4\pi\hbar^2}{15} \int_0^\infty \left[C_\parallel(\omega) + 4C_\perp(\omega) \right] I_\omega \, d\omega \tag{3.60}$$

and

$$\left\langle \left(\Delta J_{\perp}^{b}\right)^{2}\right\rangle_{abs} = \frac{4\pi\hbar^{2}}{15}\int_{0}^{\infty}\left[2C_{\parallel}(\omega)+3C_{\perp}(\omega)\right]\,I_{\omega}\,d\omega. \tag{3.61}$$

One can easily verify that in the appropriate limit expressions (3.60) and (3.61) reduce to the corresponding expression derived for spherical grains by Purcell & Spitzer (PS71, eq. 60).

3.8.3 Thermal Emission

The diffusion tensor for thermal emission can be deduced by noting that, in the hypothetical situation where the grain is immersed in a blackbody field with $T_{rad} = T_d$, the principle of detailed balancing requires that emission and absorption should contribute equally to the diffusion tensor. The components are therefore

$$\left\langle \left(\Delta J_{\parallel}^{b}\right)^{2}\right\rangle_{em} = \frac{4\pi\hbar^{2}}{15}\int_{0}^{\infty}\left[C_{\parallel}(\omega)+4C_{\perp}(\omega)\right]\,B_{\omega}(T_{d})\,d\omega. \tag{3.62}$$

and

$$\left\langle \left(\Delta J_{\perp}^{b}\right)^{2}\right\rangle_{em} = \frac{4\pi\hbar^{2}}{15}\int_{0}^{\infty}\left[2C_{\parallel}(\omega)+3C_{\perp}(\omega)\right]\,B_{\omega}(T_{d})\,d\omega, \tag{3.63}$$

where

$$B_{\omega}(T_{d}) = \frac{\omega^{2}}{4\pi^{3}c^{2}}\left[\exp\left(\hbar\omega/kT_{d}\right)-1\right]^{-1} \tag{3.64}$$

is the specific intensity of a thermal radiation field with temperature T_d.

The mean torque contributed by thermal emission can be computed using the Fluctuation-Dissipation Theorem. Thus in thermal equilibrium at temperature T_d, the damping time for rotation about the symmetry axis due to absorption *plus* emission is

$$t_{TE} = \frac{I_{zz}^{b}kT_{d}}{\left\langle \left(\Delta J_{\parallel}^{b}\right)^{2}\right\rangle_{em}}, \tag{3.65}$$

where we have used the fact that thermal emission contributes half of the total diffusion tensor in thermal equilibrium. But because the mean torques due to absorption and emission are additive, the mean torque due to emission alone must be

$$\langle\Delta\boldsymbol{J}\rangle_{em} = -\boldsymbol{J}/t_{em}, \tag{3.66}$$

where the damping time for thermal emission is related to the other time scales by

$$t_{em}^{-1} = t_{TE}^{-1} - t_{abs}^{-1}. \tag{3.67}$$

We have plotted the photoabsorption and photoemission damping times in Fig. 3 and Fig. 4, respectively, for the special but illustrative case of bare silicate grains with no ice mantles. We used the "astronomical silicate" dielectric function of Draine (1987) to compute the electric dipole absorption cross sections and chose $\rho_c = 2.5$ g cm^{-3}. We see from the figures that in clouds where $t_{gas} \leq 10^{10}$ s, the time scales t_{abs} and t_{em} are at least an order of magnitude larger than t_{gas} unless the grains have radii $b_c \ll 0.1$ μm and the radiation and dust temperatures are larger than 100 K. We conclude that photoabsorption and photoemission typically have a negligible influence on the alignment of large dielectric grains in warm clouds, but might be important in studies of polarized emission from very small, transiently-heated grains.

4 THERMAL ALIGNMENT IN MOLECULAR CLOUDS

To assess the accuracy of our numerical methods, we consider a special case— the magnetic alignment of spheres and thin disks— where our numerical results can be compared with exact analytic solutions for R. Below we include all of the processes discussed in §3 except for photoabsorption and thermal emission.

4.1 Magnetic Alignment of Core-Mantle Spheroids

The number of independent physical parameters in the Langevin equation is minimized by choosing appropriate dimensionless variables. Thus we define the dimensionless angular momentum components in the gas frame by

$$j_i \equiv \frac{J_i}{\sqrt{I_{zz}^b kT_g}}, \quad i = x, y, z, \tag{4.1}$$

and measure time in units of the gas damping time. When the diffusion coefficients from §3 are written in terms of these variables and the resulting expressions for collisions, evaporation,

and paramagnetic or super-paramagnetic absorption are added together, one finds that the total mean torque has gas frame components

$$\langle \Delta j_i \rangle = -(1+\delta)\, j_i, \quad i = x, y, \tag{4.2}$$

and

$$\langle \Delta j_z \rangle = -j_z, \tag{4.3}$$

where

$$\delta \equiv \frac{3KVB^2}{4\sqrt{\pi} n m v_{th} b_m^4 \Gamma_{\|}} \tag{4.4}$$

is the ratio t_{gas}/t_{mag} of the gas and magnetic damping times. The nonzero gas frame components of the dimensionless diffusion tensor are

$$\left\langle (\Delta j_x)^2 \right\rangle = \frac{1}{2}\left(1+\frac{T_d}{T_g}\right)\left[\left(1+\cos^2\beta\right)\frac{\Gamma_{\perp}(e_m)}{\Gamma_{\|}(e_m)} + \sin^2\beta\right] + 2\left(\frac{T_d}{T_g}\right)\delta, \tag{4.5}$$

$$\left\langle (\Delta j_y)^2 \right\rangle = \left\langle (\Delta j_x)^2 \right\rangle, \tag{4.6}$$

and

$$\left\langle (\Delta j_z)^2 \right\rangle = \left(1+\frac{T_d}{T_g}\right)\left[\sin^2\beta\,\frac{\Gamma_{\perp}(e_m)}{\Gamma_{\|}(e_m)} + \cos^2\beta\right]. \tag{4.7}$$

The coefficients which appear in the Langevin equation, eq. 2.4, can be obtained from the diffusion coefficients above via eq. (2.5)–(2.6).

According to eq. (4.2)–(4.7), the diffusion coefficients, and hence the Rayleigh reduction factor, depend only on three dimensionless parameters. These are δ, T_d/T_g, and the eccentricity of the mantle surface (which determines the ratio $\Gamma_{\perp}/\Gamma_{\|}$). Our results are identical in this respect to the earlier work of Purcell and Spitzer (PS71), even though the present work differs from PS71 in that we include Barnett relaxation and Larmor precession. Notice, however, that δ as defined in this paper differs from the quantity δ in PS71 except for the special case of spheres. This is because PS71 defined t_{gas} to be the damping time for rotation about an axis perpendicular to the grain symmetry axis. The subsequent discovery (P79) that Barnett relaxation aligns $\boldsymbol{\Omega}$ *parallel* to the symmetry axis of an oblate spheroid implies that the definition of t_{gas} adopted here is appropriate.

The symmetry of the diffusion coefficients in j_x and j_y shows that Larmor precession causes the angular momentum distribution to be axisymmetric about the the magnetic field

as expected (Martin 1971). It might seem that one could exploit this symmetry to reduce the number of coupled Langevin equations from three to two in number. For example, one might introduce the variable

$$j_\rho \equiv \sqrt{j_x^2 + j_y^2}, \tag{4.8}$$

and then evaluate

$$\langle \cos^2 \beta \rangle = \left\langle (j_\rho / j_z)^2 \right\rangle \tag{4.9}$$

by numerically computing the sample paths of j_ρ and j_z. This would amount to a change of variables in the Langevin equation. Although $\{j_i\}$ are stochastic (hence non-differentiable, cf. eq. 2.11) variables, such a change can indeed be performed if one uses "Ito's formula" from the stochastic calculus (Gardiner 1990). However, an unfortunate consequence of this procedure is that that the resulting Langevin equation for j_ρ contains a term which becomes singular when $j_\rho = 0$. While it seems likely that the Euler-Maruyama method could be modified to handle this singularity, it is not clear how much these modifications would reduce the potential computational savings— which are in any case no more than 33%— over the straightforward approach of computing j_x, j_y, and j_z. We therefore adopt the straightforward approach here.

4.2 Benchmark Calculations for Spheres and Thin Disks

Jones & Spitzer (JS67, see also PS71) obtained an exact solution for the steady-state angular momentum distribution of spheres under the influence of sticking gas-grain collisions, evaporation, and paramagnetic absorption. The applicability to this paper of the JS67 solution follows directly from the fact that our diffusion coefficients reduce to those of JS67 for spherical grains. Indeed, this correspondence is required by the fact that, for spheres, Barnett relaxation does not occur and Larmor-averaging has no effect on the diffusion coefficients for collisions and evaporation. In addition, we point out the rather surprising result that the JS67 solution is also exact for thin disks. The latter conclusion follows from the fact that R depends on the mantle eccentricity only through the ratio $\Gamma_\perp/\Gamma_\parallel$ (cf. eq. 4.4–4.7), and this ratio is unity for both $e_m = 0$ and $e_m = 1$ (cf. eq. 3.37–3.38). Thus, a thin disk and sphere will be aligned with equal efficiency for equal values of the parameters δ and T_d/T_g.[5]

[5] Of course this does not imply that spheres and thin disks will be aligned equally under a given set of *physical conditions*. The parameter δ is proportional to the grain volume, V, which is zero if $e_m = 1$. Thus the magnetic alignment of an infinitely thin disk is always zero and, in this sense, the exact solution for thin disks is only of academic interest. However, $\Gamma_\perp/\Gamma_\parallel$ never differs from unity by more than about 15% (Fig. 2), suggesting that the exact solution for spheres and disks may furnish a good approximation for grains of all intermediate eccentricities. This possiblity is explored in the numerical calculations presented in Paper II.

Although we will ultimately be interested only in the steady-state angular momentum distribution, it is useful to consider the time-dependent distribution, $f(\boldsymbol{J}, t)$, for the purpose of estimating various time scales of interest. It is possible to find exact, time-dependent solutions which satisfy various initial conditions and which reduce to the JS67 solution as $t \rightarrow \infty$. Here we will consider an arbitrary but representative example where

$$j_i(0) = 0, \quad i = x, y, z, \tag{4.10}$$

i.e., where the initial conditions are deterministic with the grains initially at rest. One can easily show that the FP equation is satisfied if the distribution of each component, j_i, is a statistically independent Gaussian with zero mean value. The time-dependence enters via the variances, which are

$$\sigma_x^2 = \sigma_y^2 = \frac{1 + (1 + 2\delta)(T_d/T_g)}{2(1 + \delta)} \left\{1 - \exp\left[-2(1 + \delta)\tau\right]\right\}, \tag{4.11}$$

for the components normal to $\boldsymbol{B}$ and

$$\sigma_z^2 = \frac{1 + (T_d/T_g)}{2} \left\{1 - \exp(-2\tau)\right\} \tag{4.12}$$

for the component parallel to $\boldsymbol{B}$, where τ is dimensionless time in units of t_{gas}. Thus the distributions of j_x and j_y relax to a steady state on a time scale of order $t_{gas}/(1 + \delta)$ while the corresponding relaxation time for j_z is t_{gas}. The relaxation time is evidently just the time scale on which rotational drag causes a grain to "forget" its initial angular momentum; this time scale is determined by gas drag alone for the component parallel to $\boldsymbol{B}$ and by gas

drag plus paramagnetic absorption for the components perpendicular to $\boldsymbol{B}$. In the following discussion, the term "relaxation time" will refer specifically to t_{gas}, i.e. to the larger of the two relaxation times above. Henceforth we consider only the stationary distribution on the assumption that the gas and grain properties are constant over time scales $\lesssim t_{gas}$ (Table 1).

In a steady state, the statistic $\langle \cos^2 \beta \rangle$ on which R depends is given exactly by

$$\langle \cos^2 \beta \rangle = \begin{cases} \frac{1}{x}\left[\left(\frac{1+x}{x}\right)^{1/2} \sinh^{-1} x^{1/2} - 1\right], & \text{if } x > 0 \\ \\ \frac{1}{x}\left[\left(\frac{1+x}{-x}\right)^{1/2} \sin^{-1}(-x)^{1/2} - 1\right], & \text{if } x < 0 \end{cases} \tag{4.13}$$

where

$$x \equiv \sigma_x^2/\sigma_z^2 - 1 \tag{4.14}$$

(cf. PS71, eq. 23). The steady state autocorrelation function of $j_i(\tau)$ can be shown to be

$$\langle j_i(\tau)\, j_i(\tau') \rangle = \sigma_i^2 \exp\left[-|\tau - \tau'|/\tau_{cor,i}\right], \tag{4.15}$$

where the dimensionless correlation times in units of t_{gas} are given by

$$\tau_{cor,i} = \begin{cases} \frac{1}{1+\delta} & \text{if } i = x, y \\ \\ 1 & \text{if } i = z. \end{cases} \tag{4.16}$$

Henceforth, we will take the term "correlation time," to mean the smaller of these time scales, i.e.

$$\tau_{cor} \equiv \frac{1}{1+\delta}. \tag{4.17}$$

We expect, rougly speaking, that the minimum time scale for fluctuations in $\cos^2 \beta$ will be of order τ_{cor}.

Numerical estimates of $\langle \cos^2 \beta \rangle$ for spheres and disks were obtained for comparison with exact solutions as follows. Given values of the parameters δ and T_d/T_g, we calculated $N = 50$ values of $\langle \cos^2 \beta \rangle$ from N identical trial calculations. In each trial, we took the initial conditions as in eq. (4.10) and then used the Euler-Maruyama scheme, eq. (2.14), to generate a sample path of $\boldsymbol{j}(t)$. The Box-Muller algorithm was used to generate the Wiener increments

from a sequence of uniform pseudo-random numbers and the latter were obtained, in turn, using the portable random number generator referred to as "RAN3" in Press et al. (1986). In each trial, we integrated the sample path initially for 100 relaxation times to let the grain forget its initial conditions. Thereafter the time averaging of $\cos^2\beta$ commenced and the Langevin equation was integrated over an additional, dimensionless "averaging time," τ_{avg}. The error in each trial integration was characterized by E_{rel}, the relative error in $\langle\cos^2\beta\rangle$ determined by comparing the trial result with the exact solution. We expect the accuracy of $\langle\cos^2\beta\rangle$ to depend on τ_{avg}, on the dimensionless time step, $\Delta\tau$, and on systematic errors caused by various effects such as spurious correlations in the random number generator. We now consider each of these effects individually.

The dependence of errors on the averaging time is illustrated in Figure 5, where we have plotted the root-mean-square value of the $N = 50$ values of E_{rel} as a function of τ_{avg}. All of the calculations in Fig. 5 pertain to spheres or thin disks with $T_d/T_g = 0.5$, $\delta = 1$, and used a time step $\Delta\tau = 1 \times 10^{-3}\tau_{cor}$. The straight line in Fig. 5 is a least squares fit to the plotted points. Its slope, -0.47, is consistent to within the statistical errors in E_{rms} with the scaling law $E_{rms} \propto (\tau_{avg}/\tau_{cor})^{-1/2}$. Of course this is just the scaling one expects on the basis of the Central Limit Theorem: the value of $\langle\cos^2\beta\rangle$ at the end of a trial is effectively the mean of M statistically independent estimates, where each independent estimate corresponds to the average over one correlation time and $M = \tau_{avg}/\tau_{cor}$ is the number of correlation times in one trial integration.

The dependence of E_{rms} on the time step is shown in Fig. 6. Each rms error was determined as in Fig. 5 from the results of 50 identical trial integrations. The total integration time for all points in Fig. 6 was $\tau_{avg} = 5 \times 10^4\tau_{cor}$ and the physical parameters were chosen to be $\delta = 1$, $T_d/T_g = 0.5$. For large $\Delta\tau$, where the accuracy in $\langle\cos^2\beta\rangle$ is limited primarily by the time step, E_{rms} scales approximately as $(\Delta\tau/\tau_{cor})^{-m}$, where $m \approx 1$. As $\Delta\tau$ decreases, the rms error approaches a constant, reflecting the fact that the accuracy in $\langle\cos^2\beta\rangle$ is eventually limited by the integration time. Thus the minimum useful time step is about $\Delta\tau = 10^{-2}$ for an integration time of $\tau_{avg} = 5 \times 10^4\tau_{cor}$. Note that the slight upturn in E_{rms} for the smallest time step, $\Delta\tau = 1 \times 10^{-3}\tau_{cor}$, is not statistically significant: The increase in log E_{rms}, about

0.05, is approximately equal to $1/\sqrt{N}$, where $N = 50$ is the number of independent trials used to determine E_{rms}. That is, the upturn is only a "1σ" fluctuation.

Systematic errors due to spurious correlations in the random numbers, etc, should reveal themselves as residual mean errors in calculations where the two effects discussed above are small. An upper limit on any systematic errors which may be present in our numerical results can be inferred from the data in Figures 7 and 8. The histograms depict the distributions in E_{rel} for $N = 100$ identical trials with $\Delta\tau/\tau_{cor} = 1.0\times10^{-3}$ and two different integration times. All of the calculations in Fig. 7 and 8 pertain to the case $\delta = 3$ and $T_d/T_g = 0.9$. In Fig. 7, where $\tau_{avg} = 6 \times 10^4 \tau_{cor}$, the relative errors have mean value $\overline{E}_{rel} = -1 \times 10^{-3}$ and standard deviation $\sigma_E = 5 \times 10^{-3}$. In Fig. 8, where $\tau_{avg} = 1 \times 10^6 \tau_{corr}$, the corresponding statistics are $\overline{E}_{rel} = -6 \times 10^{-6}$ and $\sigma_E = 1 \times 10^{-3}$. We conclude from the smallness of $\left|\overline{E}_{rel}\right| / \sigma_E$ that any systematic errors which may be present are much smaller than the statistical errors. The "production calculations" presented in Paper II use a time step of $\Delta\tau = 1 \times 10^{-3}\tau_{cor}$ and an integration time of $\tau_{avg} = 6 \times 10^4 \tau_{cor}$[6]. The histogram in Fig. 7 therefore reflects the distribution of relative errors in our production runs. We conclude that our production calculations have a 2σ error in $\langle\cos^2\beta\rangle$ of about 2%, which translates to a 2σ error in R of about 6% when $R = 0.1$. When $R \ll 0.1$, the relative error in R is generally much larger than 6% because $\langle\cos^2\beta\rangle \approx 1/3$ (cf. eq. [1.1]). This effect is shown in Fig. 9, where the symbols depict R-values for spherical grains determined by numerical integration and the solid curves give the exact analytic solutions for comparison. The rms error in R (not $\log R$) for all points in Fig. 9 is 1.3% but the point with $R = 5 \times 10^{-3}$ has an error of about 25%. We could reduce the errors in very small R values somewhat by integrating longer and with a smaller time step, but there does not appear to be any incentive for doing so at present. The 25% error in $R = 5 \times 10^{-3}$ is an extreme example which, in any case, has no observable consequences. For example, the linear polarization in far-infrared or submillimeter emission from aligned, oblate spheroids made of astronomical silicates (Draine 1987) would be about

[6] The reader may notice that our integration time does not warrant such a small time step (cf. Fig. 6). We choose a small time step to allow for the possibility of averaging our results with additional integrations if computer time becomes more plentiful in the future.

$60R\%$ for an axis ratio $b_m/a_m = 2$ if we neglected (unrealistically) effects which reduce the effective degree of alignment, such magnetic field line inhomogeneities along the line of sight. Even in this optimistic picture, the polarization corresponding to $R = 5 \times 10^{-3}$ would be near the limit of detectability (e.g., Hildebrand et al. 1992) and a 25% error in R would be unobservable in this case.

5 SUMMARY

1. We have demonstrated a new method for obtaining accurate predictions of grain alignment theories which uses numerical integration of the Langevin equation. The new method is easy to implement and superior in several respects to Monte Carlo techniques or the direct solution of the Fokker-Planck equation.

2. We have calculated the Fokker-Planck diffusion coefficients for physical processes relevant to super-paramagnetic grain alignment in molecular clouds, on the *ad hoc* hypothesis that the grains do not rotate suprathermally. These calculations will be applied in the next paper of this series to derive observational tests of this hypothesis.

3. We have developed a quantitative theory for the effects of thermal emission and far-infrared absorption on the alignment of nonspherical, dielectric grains. These processes generally have a negligible effect on grain alignment in molecular clouds.

4. We have performed benchmark calculations to calibrate the errors in our computational methods. We have determined the dependence of errors in the Rayleigh reduction factor on parameters in our numerical integration scheme. Any systematic errors that may be present in our calculations correspond to spurious predictions of nonzero alignment which are below the present limits of detectability.

ACKNOWLEDGEMENTS

We are indebted to Drs. Daniel Sperber and Joseph Haus, Rensselaer, for pointing out the equivalence between the Fokker-Planck and Langevin equations. We thank Dr. Bruce Draine, Princeton U., for providing a numerical tabulation of the grain optical properties

in Draine (1987) and Dr. Kathryn Mead, Union College, for generously providing computing resources. This work was supported by the NASA Infrared, Submillimeter, and Radio Astronomy Program under Grant NAGW-3001.

APPENDIX A
STICKING COLLISIONS ON AN INFINITESIMAL SURFACE PATCH

We compute the incremental contributions to the mean torque and diffusion tensor which are caused by sticking collisions onto an infinitesimal surface patch of the grain. The results of this appendix apply to grains with arbitrary shapes, angular velocities, and gas-grain drift velocities. (The effects of gas-grain drift are included for reference in future work.) The incremental contributions are integrated over the surface of an oblate spheroid in Appendix C to obtain the total diffusion coefficients for sticking collisions.

A.1 Differential Flux of Colliding Molecules

Let $\boldsymbol{v} = v_{th}\,\boldsymbol{s}$ be the velocity of a molecule in the gas frame (i.e., its thermal velocity), where $\boldsymbol{s}$ is dimensionless and

$$v_{th} \equiv \left(\frac{2kT_g}{m}\right)^{1/2} \tag{A1}$$

is the gas thermal speed. If the distribution of thermal velocities is Maxwellian at the gas temperature, then the mean flux of colliding particles with velocities in the range $(\boldsymbol{s}, \boldsymbol{s}+d^3\boldsymbol{s})$ is $nv_{th}\,f_c(\boldsymbol{s})\,d^3\boldsymbol{s}$, where

$$f_c(\boldsymbol{s}) = \begin{cases} \pi^{-3/2}\,(\boldsymbol{s}_p - \boldsymbol{s})\cdot\hat{n}\,\exp\left(-s^2\right) & \text{if } (\boldsymbol{s}-\boldsymbol{s}_p)\cdot\hat{n} < 0 \\ 0 & \text{otherwise} \end{cases} \tag{A2}$$

and

$$\boldsymbol{s}_p \equiv \left(\boldsymbol{v}_d + \boldsymbol{\Omega}\times\boldsymbol{r}\right)/v_{th} \tag{A3}$$

is the total translational plus rotational velocity of the patch in the gas frame in units of v_{th}.

A.2 Incremental Mean Torque

Consider an infinitesimal surface patch of the grain with area dA, unit outward normal $\hat{n}$, and position vector $\boldsymbol{r}$ relative to the grain CM. When a molecule with velocity $v_{th}\,\boldsymbol{s}$ sticks

to the patch, the grain internal angular momentum increases by

$$\delta \boldsymbol{J}(\boldsymbol{s}) = m v_{th} \left[\boldsymbol{r} \times (\boldsymbol{s} - \boldsymbol{s}_d) \right], \tag{A4}$$

where $\boldsymbol{v}_d = v_{th} \boldsymbol{s}_d$ is the CM velocity of the grain in the gas frame. Multiplying expression (A4) by the mean flux of colliding particles and then integrating over all thermal velocities gives the patch's contribution to the mean torque due to sticking collisions. Its cartesian components are

$$d \langle \Delta J_i \rangle_c = n \, v_{th} \, dA \int \delta J_i(\boldsymbol{s}) \, f_c(\boldsymbol{s}) \, d^3 \boldsymbol{s}, \tag{A5}$$

where in this and subsequent expressions integrals over $\boldsymbol{s}$ are assumed to be definite integrals over all of $\boldsymbol{s}$-space. The integral in eq. (A5) can be evaluated analytically to give

$$d \langle \Delta J_i \rangle_c = n \, m \, v_{th}^2 \; \left[G(\boldsymbol{s}_p \cdot \hat{\boldsymbol{n}}) \, (\boldsymbol{r} \times \hat{\boldsymbol{n}})_i \; - \; F(\boldsymbol{s}_p \cdot \hat{\boldsymbol{n}}) \, (\boldsymbol{r} \times \boldsymbol{s}_d)_i \right] \, dA, \tag{A6}$$

where the functions F and G are defined below in §A.4.

A.3 Incremental Diffusion Tensor

The patch's incremental contribution to the diffusion tensor has cartesian components

$$d \langle \Delta J_i \, \Delta J_j \rangle_c = n \, v_{th} \, dA \int \delta J_i(\boldsymbol{s}) \, \delta J_j(\boldsymbol{s}) \, f_c(\boldsymbol{s}) \, d^3 \boldsymbol{s}. \tag{A7}$$

The integral can be evaluated analytically by straighforward calculation to show that

$$d \langle \Delta J_i \, \Delta J_j \rangle_c = \sum_{k=1}^{4} d \langle \Delta J_i \, \Delta J_j \rangle_c^{(k)}, \tag{A8}$$

where

$$d \langle \Delta J_i \, \Delta J_j \rangle_c^{(1)} = \tfrac{1}{2} n m^2 v_{th}^3 F(\boldsymbol{s}_p \cdot \hat{\boldsymbol{n}}) \mathcal{T}_{ij}^{(1)} dA, \tag{A9}$$

$$d \langle \Delta J_i \, \Delta J_j \rangle_c^{(2)} = n m^2 v_{th}^3 \left[H(\boldsymbol{s}_p \cdot \hat{\boldsymbol{n}}) - \tfrac{1}{2} F(\boldsymbol{s}_p \cdot \hat{\boldsymbol{n}}) \right] \mathcal{T}_{ij}^{(2)} dA, \tag{A10}$$

$$d \langle \Delta J_i \, \Delta J_j \rangle_c^{(3)} = -n m^2 v_{th}^3 G(\boldsymbol{s}_p \cdot \hat{\boldsymbol{n}}) \mathcal{T}_{ij}^{(3)} dA, \tag{A11}$$

and

$$d\,\langle \Delta J_i\, \Delta J_j \rangle_c^{(4)} = nm^2 v_{th}^3 F(\boldsymbol{s}_p \cdot \hat{n}) \mathcal{T}_{ij}^{(4)} dA. \tag{A12}$$

The function H is defined below and $\mathcal{T}^{(1)}, \ldots, \mathcal{T}^{(4)}$ are second-rank tensors with components

$$\mathcal{T}_{ij}^{(1)} \equiv r^2\, \delta_{ij} - r_i r_j, \tag{A13}$$

$$\mathcal{T}_{ij}^{(2)} \equiv (\boldsymbol{r} \times \hat{n})_i (\boldsymbol{r} \times \hat{n})_j, \tag{A14}$$

$$\mathcal{T}_{ij}^{(3)} \equiv (\boldsymbol{r} \times \hat{n})_i (\boldsymbol{r} \times \boldsymbol{s}_d)_j + (\boldsymbol{r} \times \boldsymbol{s}_d)_i (\boldsymbol{r} \times \hat{n})_j, \tag{A15}$$

and

$$\mathcal{T}_{ij}^{(4)} \equiv (\boldsymbol{r} \times \boldsymbol{s}_d)_i (\boldsymbol{r} \times \boldsymbol{s}_d)_j, \tag{A16}$$

where δ_{ij} is the Kronecker delta symbol.

A.4 Special Functions

The function

$$F(x) \equiv \frac{1}{2}\left[x\,(1 + \operatorname{erf} x) + \frac{1}{\sqrt{\pi}} \exp\left(-x^2\right)\right] \tag{A17}$$

is just the dimensionless particle flux integrated over all thermal velocities for a patch whose velocity in the gas frame has a component $x = \boldsymbol{s}_p \cdot \hat{n}$ along its own outward normal. The limiting behavior of F for large and small $|x|$ is

$$F(x) \longrightarrow \begin{cases} \frac{1}{4\sqrt{\pi}}\, x^{-2} \exp\left(-x^2\right) & x \to -\infty \\ \\ \frac{1}{2\sqrt{\pi}} + \frac{1}{2} x & x \to 0 \\ \\ x + \frac{1}{4\sqrt{\pi}}\, x^{-2} \exp\left(-x^2\right) & x \to +\infty. \end{cases} \tag{A18}$$

The function

$$G(x) \equiv -\frac{1}{4}\left[1 + \frac{|x|}{x} P\left(\tfrac{3}{2}, x^2\right)\right] - \frac{x}{2\sqrt{\pi}} \exp\left(-x^2\right) \tag{A19}$$

is defined in terms of the incomplete gamma function,

$$P(a, u) \equiv \frac{1}{\Gamma(a)} \int_0^u t^{a-1} \exp(-t)\, dt, \tag{A20}$$

and has the limiting forms

$$G(x) \longrightarrow \begin{cases} \frac{1}{4x\sqrt{\pi}} \exp(-x^2) & x \to -\infty \\ -\frac{1}{4} - \frac{x}{2\sqrt{\pi}} & x \to 0 \\ -\frac{1}{2} + \frac{1}{4x\sqrt{\pi}} \exp(-x^2) & x \to +\infty. \end{cases} \tag{A21}$$

The function

$$H(x) \equiv \frac{1}{4} x \left[1 + \frac{|x|}{x} P\left(\frac{3}{2}, x^2\right)\right] + \frac{1}{2\sqrt{\pi}} (1 + x^2) \exp(-x^2) \tag{A22}$$

has the limiting behavior

$$H(x) \longrightarrow \begin{cases} \frac{1}{4\sqrt{\pi}} \exp(-x^2) & x \to -\infty \\ \frac{1}{2\sqrt{\pi}} + \frac{1}{4}x & x \to 0 \\ \frac{1}{2}x + \frac{1}{4\sqrt{\pi}} \exp(-x^2) & x \to +\infty. \end{cases} \tag{A23}$$

APPENDIX B
THERMAL EVAPORATION FROM AN INFINITESIMAL SURFACE PATCH

Here we compute the contribution of an infinitesimal surface patch to the diffusion coefficients for thermal evaporation. The results of this appendix apply to grains with arbitrary shapes, angular velocities, and gas-grain drift velocities. The total diffusion coefficients for thermal evaporation from an oblate spheroid are derived in Appendix C by integrating the results of this appendix over the grain surface.

B.1 Differential Flux of Evaporating Molecules

Let $\boldsymbol{v}' = v_{ev}\,\boldsymbol{s}'$ be the velocity of an evaporating molecule in the frame of reference of the surface patch, where $\boldsymbol{s}'$ is dimensionless and

$$v_{ev} \equiv \left(\frac{2kT_d}{m}\right)^{1/2} \tag{B1}$$

is a characteristic thermal speed for evaporation. Consider first the hypothetical situation where the gas and grain temperatures are equal and the patch is at rest in the gas frame. In this special case, the principle of detailed balancing requires that every evaporation with velocity $\boldsymbol{v}'$ should be accompanied, on average, by a sticking collision with velocity $-\boldsymbol{v}'$. The velocity distribution of evaporating molecules is therefore proportional to

$$f_{ev}(\boldsymbol{s}') = \begin{cases} \frac{2}{\pi}\,\boldsymbol{s}'\cdot\hat{\boldsymbol{n}}\,\exp\left[-(s')^2\right] & \text{if } \boldsymbol{s}'\cdot\hat{\boldsymbol{n}} > 0 \\ \\ 0 & \text{otherwise,} \end{cases} \tag{B2}$$

which is equal, apart from a normalization factor discussed below, to the flux of sticking collisions, eq. (A2), with $\boldsymbol{s}' = -\boldsymbol{s}$ and the patch velocity, $\boldsymbol{s}_p$, set to zero. Although it was derived assuming that $T_d = T_g$, expression (B2) is correct for all T_d and T_g because the evaporation spectrum is obviously independent of the gas temperature. We will also assume that expression (B2) is correct for a *rotating* surface patch. The neglect of any possible dynamical coupling between grain rotation and evaporation should be an excellent approximation for grains rotating at thermal angular velocities, because the centrifugal potential of a molecule

rotating along with the grain surface is only of order $(m/M_d)\,kT_g$. We have defined f_{ev} to be normalized so that

$$\int f_{ev}(\boldsymbol{s}')\,d^3\boldsymbol{s}' = 1, \tag{B3}$$

where in this and subsequent expressions it is assumed that integration over $\boldsymbol{s}'$ means integration over all of $\boldsymbol{s}'$-space. The differential flux is therefore $\bar{\Phi}\,f_{ev}(\boldsymbol{s}')$, where $\bar{\Phi}$ is the mean number of evaporations $\mathrm{cm}^{-2}\ \mathrm{s}^{-1}$ integrated over all $\boldsymbol{s}'$. If the evaporation rate is independent of position on the grain surface, which is the case of interest in this paper where suprathermal rotation is not considered, then $\bar{\Phi}$ is set by the requirement that the total collision and evaporation rates integrated over the surface must balance. Thus

$$\bar{\Phi} = \frac{n v_{th} \int F(\boldsymbol{s}_p\cdot\hat{\boldsymbol{n}})\,dA}{S}, \tag{B4}$$

where v_{th} is the *gas* thermal speed, S is the total grain surface area, the integral is over the grain surface, and the function $F(\boldsymbol{s}_p\cdot\hat{\boldsymbol{n}})$ is defined in Appendix A.

B.2 Incremental Mean Torque

A molecule which evaporates with dimensionless velocity $\boldsymbol{s}'$ relative to the rotating, drifting grain surface has a (dimensional) velocity

$$\boldsymbol{v} = v_{ev}\boldsymbol{s}' + \boldsymbol{\Omega}\times\boldsymbol{r} \tag{B5}$$

relative to the grain CM and its departure changes the grain internal angular momentum by

$$\delta\boldsymbol{J}(\boldsymbol{s}') = -m\left\{ v_{ev}\,(\boldsymbol{r}\times\boldsymbol{s}') + \boldsymbol{r}\times(\boldsymbol{\Omega}\times\boldsymbol{r})\right\}. \tag{B6}$$

The incremental mean torque due to evaporation from a single surface patch therefore has cartesian components

$$d\left\langle\Delta J_i\right\rangle_{ev} = \bar{\Phi}\,dA \int \delta J_i(\boldsymbol{s}')\ f_{ev}(\boldsymbol{s}')\,d\boldsymbol{s}'. \tag{B7}$$

Straightforward evaluation of the integral above shows that

$$d\left\langle\Delta J_i\right\rangle_{ev} = -m\,\bar{\Phi}\left\{ \frac{\sqrt{\pi}}{2} v_{ev}\,(\boldsymbol{r}\times\hat{\boldsymbol{n}})_i \ +\ \left(\boldsymbol{\mathcal{T}}^{(1)}\cdot\boldsymbol{\Omega}\right)_i \right\} dA, \tag{B8}$$

where $\left(\boldsymbol{\mathcal{T}}^{(1)}\cdot\boldsymbol{\Omega}\right)$ denotes the scalar product of $\boldsymbol{\Omega}$ with the second-rank tensor $\boldsymbol{\mathcal{T}}^{(1)}$ (cf. Appendix A).

B.3 Incremental Diffusion Tensor

The patch's incremental contribution to the diffusion tensor has cartesian components

$$d\,\langle \Delta J_i\, \Delta J_j \rangle_{ev} = \bar{\Phi}\, dA \int \delta J_i(\boldsymbol{s}')\, \delta J_j(\boldsymbol{s}')\, f_{ev}(\boldsymbol{s}')\, d\boldsymbol{s}'. \tag{B9}$$

When the integration over $\boldsymbol{s}'$ is performed, the cartesian components are found to be

$$d\,\langle \Delta J_i\, \Delta J_j \rangle_{ev} = \sum_{k=1}^{3} d\,\langle \Delta J_i\, \Delta J_j \rangle_{ev}^{(k)}, \tag{B10}$$

where

$$d\,\langle \Delta J_i\, \Delta J_j \rangle_{ev}^{(1)} = \frac{1}{2} m^2 v_{ev}^2 \bar{\Phi} \left[\mathcal{T}_{ij}^{(1)} + \mathcal{T}_{ij}^{(2)} \right] dA, \tag{B11}$$

$$d\,\langle \Delta J_i\, \Delta J_j \rangle_{ev}^{(2)} = \frac{\sqrt{\pi}}{2} m^2 v_{ev} \bar{\Phi} \left[(\boldsymbol{r} \times \hat{n})_i \left(\mathcal{T}^{(1)} \cdot \boldsymbol{\Omega} \right)_j + \left(\mathcal{T}^{(1)} \cdot \boldsymbol{\Omega} \right)_i (\boldsymbol{r} \times \hat{n})_j \right] dA, \tag{B12}$$

and

$$d\,\langle \Delta J_i\, \Delta J_j \rangle_{ev}^{(3)} = m^2 \bar{\Phi} \left(\mathcal{T}^{(1)} \cdot \boldsymbol{\Omega} \right)_i \left(\mathcal{T}^{(1)} \cdot \boldsymbol{\Omega} \right)_j dA. \tag{B13}$$

APPENDIX C
DIFFUSION COEFFICIENTS FOR STICKING COLLISIONS AND EVAPORATION FROM AN OBLATE SPHEROID

C.1 Oblate Spheroidal Coordinates

Here we compute the diffusion coefficients for sticking collisions and thermal evaporation by integrating the incremental diffusion coefficients from Appendixes A–B over the surface of an oblate spheroid. In the present paper we will assume that the grain center of mass is at rest in the gas frame ($\boldsymbol{v}_d = 0$) and that the grain is rotating about its symmetry axis due to the effects of internal dissipation. The surface integrals are easy to evaluate if one specifies the position of a surface element by its oblate spheroidal coordinates, (η, ξ), where $\eta \in [-\pi/2, \pi/2]$ and $\xi \in [0, 2\pi]$ (see, e.g., Arfken 1970). Thus the vector $\boldsymbol{r}(\eta, \xi)$ from the grain CM to the mantle surface at (η, ξ) has body-frame coordinates

$$\begin{aligned} x^b(\eta,\xi) &= b_m \cos\eta \, \cos\xi \\ y^b(\eta,\xi) &= b_m \cos\eta \, \sin\xi \\ z^b(\eta,\xi) &= a_m \sin\eta. \end{aligned} \tag{C1}$$

The length of $\boldsymbol{r}$ is

$$r(\eta,\xi) = b_m \left[\cos^2\eta \; + \; (1-e_m^2)\sin^2\eta\right]^{1/2}, \tag{C2}$$

the unit outward normal to the surface at $\boldsymbol{r}$ has body-frame coordinates

$$\begin{aligned} \hat{n}_x^b(\eta,\xi) &= \left[\sin^2\eta + (1-e_m^2)\cos^2\eta\right]^{-1/2} (1-e_m^2)^{1/2} \cos\eta \, \cos\xi \\ \hat{n}_y^b(\eta,\xi) &= \left[\sin^2\eta + (1-e_m^2)\cos^2\eta\right]^{-1/2} (1-e_m^2)^{1/2} \cos\eta \, \sin\xi \\ \hat{n}_z^b(\eta,\xi) &= \left[\sin^2\eta + (1-e_m^2)\cos^2\eta\right]^{-1/2} \sin\eta, \end{aligned} \tag{C3}$$

and the differential element of surface area is

$$dA(\eta,\xi) = e_m \, b_m^2 \left[\frac{(1-e_m^2)}{e_m^2} + \sin^2\eta\right]^{1/2} \cos\eta \, d\eta \, d\xi. \tag{C4}$$

C.2 Sticking Collisions

C.2.1 Mean Torque

The mean torque is obtained by using expressions (C1)–(C4) to write the incremental diffusion tensor of a surface patch, eq. (A6), as a function of its oblate spheroidal coordinates and then integrating over η and ξ. First we note that $\boldsymbol{s}_p \cdot \hat{n} = 0$ everywhere on the mantle surface because $\boldsymbol{v}_d = 0$ and the grain is a surface of revolution which is rotating about its symmetry axis. Noting also that the second term in (A6) vanishes when $\boldsymbol{v}_d = 0$, and that $G(\boldsymbol{s}_p \cdot \hat{n}) = G(0) = -1/4$ is just a constant, we see that the mean torque due to collisions has cartesian, body-frame components

$$\left\langle \Delta J_i^b \right\rangle_c = -\frac{1}{4} n m v_{th}^2 \int (\boldsymbol{r} \times \hat{n})_i^b \, dA. \tag{C5}$$

The integral above vanishes for any surface of revolution. We conclude in agreement with PS71 that the mean torque due to sticking collisions is zero,

$$\left\langle \Delta J_i^b \right\rangle_c = 0, \tag{C6}$$

for any surface of revolution which is rotating about its symmetry axis.

C.2.2 Diffusion Tensor

To integrate expression (A8) over the grain surface, we first make use of the fact that $\boldsymbol{s}_d = 0$ and $\boldsymbol{s}_p \cdot \hat{n} = 0$ as noted above, from which it follows that two of the tensors in (A8) vanish,

$$\mathcal{T}^{(3)} = \mathcal{T}^{(4)} = 0, \tag{C7}$$

and also that the functions

$$F(\boldsymbol{s}_p \cdot \hat{n}) = \frac{1}{2\sqrt{\pi}} \tag{C8}$$

and

$$H(\boldsymbol{s}_p \cdot \hat{n}) = \frac{1}{2\sqrt{\pi}} \tag{C9}$$

are just constants. The diffusion tensor for sticking collisions therefore has body-frame components given by the surface integral

$$\left\langle \Delta J_i^b \, \Delta J_j^b \right\rangle_c = \frac{1}{4\sqrt{\pi}} n m^2 v_{th}^3 \int \left\{ \mathcal{T}_{ij}^{(1,b)}(\eta, \xi) + \mathcal{T}_{ij}^{(2,b)}(\eta, \xi) \right\} \, dA(\eta, \xi). \tag{C10}$$

The integrals can be evaluated analytically for each i and j by first writing out the tensor components as functions of (η, ξ) using eq. (C1) and (C3). Straightforward calculation shows that $\left\langle \Delta J_i^b \, \Delta J_j^b \right\rangle_c$ is diagonal with components

$$\left\langle (\Delta J_{\|}^b)^2 \right\rangle_c = \frac{2\sqrt{\pi}}{3} n m^2 b_m^4 v_{th}^3 \Gamma_{\|}(e_m) \tag{C11}$$

and

$$\left\langle (\Delta J_{\perp}^b)^2 \right\rangle_c = \frac{2\sqrt{\pi}}{3} n m^2 b_m^4 v_{th}^3 \Gamma_{\perp}(e_m), \tag{C12}$$

where the subscripts "$\|$" and "$\perp$," respectively, denote body frame axes parallel and normal to the symmetry axis. The shape dependence of the diffusion tensor is expressed in the functions

$$\Gamma_{\|}(e_m) \equiv \frac{3}{16} \left\{ 3 + 4(1 - e_m^2) g(e_m) - e_m^{-2} \left[1 - (1 - e_m^2)^2 g(e_m) \right] \right\}, \tag{C13}$$

and

$$\Gamma_{\perp}(e_m) = \frac{3}{32} \left\{ 7 - e_m^2 + (1 - e_m^4) g(e_m) + (1 - 2e_m^2) \left[1 + e_m^{-2} \left[1 - (1 - e_m^2)^2 g(e_m) \right] \right] \right\}, \tag{C14}$$

where

$$g(e_m) \equiv \frac{1}{2e_m} \ln \left(\frac{1 + e_m}{1 - e_m} \right). \tag{C15}$$

C.3 Thermal Evaporation

C.3.1 Mean Torque

The integration of the incremental mean torque over the mantle surface is simplified by noting that, because $\boldsymbol{s}_p \cdot \hat{\boldsymbol{n}} = 0$ everywhere on the surface, the mean evaporation flux is just

$$\bar{\Phi} = \frac{n v_{th}}{2\sqrt{\pi}}. \tag{C16}$$

The first term in eq. (B8) vanishes when integrated over the mantle surface as noted above. Integration of the remaining term shows that

$$\begin{aligned} \left\langle \Delta J_x^b \right\rangle_{ev} &= 0 \\ \left\langle \Delta J_y^b \right\rangle_{ev} &= 0 \\ \left\langle \Delta J_z^b \right\rangle_{ev} &= -\tfrac{4\sqrt{\pi}}{3} n m v_{th} b_m^4 \Gamma_{\|}(e_m) \Omega, \end{aligned} \tag{C17}$$

where we used the fact that $\boldsymbol{\Omega} = \Omega \hat{z}^b$ due to the effects of internal dissipation. Thus

$$\langle \Delta J \rangle_{ev} = -\boldsymbol{J}/t_{gas}, \tag{C18}$$

where the gas damping time is defined to be

$$t_{gas} \equiv \frac{3}{4\sqrt{\pi}} \frac{I_{zz}^b}{n m v_{th} b_m^4 \Gamma_{\|}(e_m)} \tag{C19}$$

and we have dropped the superscript "b" in eq. (C18) because it is written in a form which is valid in any coordinate system.

C.3.2 Diffusion Tensor

Our assumption that the grain rotational energy is of order kT_g implies that magnitudes of expressions (B11), (B12), and (B13) are in the approximate ratio $1{:}\sqrt{m/M_d}{:}m/M_d$. Thus the diffusion tensor for evaporation is approximately

$$\left\langle \Delta J_i^b \Delta J_j^b \right\rangle_{ev} = \frac{1}{4\sqrt{\pi}} n\, m^2\, v_{th} v_{ev}^2 \int \left\{ \mathcal{T}_{ij}^{(1,b)}(\eta,\xi) + \mathcal{T}_{ij}^{(2,b)}(\eta,\xi) \right\} dA(\eta,\xi), \tag{C20}$$

where, in neglecting the contributions due to expressions (B12) and (B13), we have introduced a relative error which is typically of order 10^{-4} for large grains with $b_m \gtrsim 0.1$ μm. Comparing eq. (C20) with eq. (C10), we see that the diffusion tensors for collisions and evaporation are related by

$$\left\langle \Delta J_i^b \Delta J_j^b \right\rangle_{ev} = \frac{T_d}{T_g} \left\langle \Delta J_i^b \Delta J_j^b \right\rangle_{c}. \tag{C21}$$

This result also could have been deduced from the principle of detailed balance (see, e.g., JS67), i.e. without performing the integration in eq. (C20). We derived expression (C21) directly as a check on the complicated series of calculations which yielded the diffusion tensor for collisions.

Table 1

Time Scales for an Oblate Spheroidal Grain[a]

Symbol	Definition	Value
t_{rot}	Grain Rotation Period	$6.3 \times 10^{-5}\ T_{g,1}^{-1/2}\, a_{m,-5}^{1/2}\, b_{m,-5}^{2}\, \Theta_{zz}^{1/2}$
t_{lar}	Larmor Precession Period	$3.7 \times 10^{5}\ B_{-5}^{-1}\, \left(\chi'_{-3}\right)^{-1}\, b_{m,-5}^{2}\, \Theta_{zz}$
t_{bar}	Barnett Relaxation Time	$3.3 \times 10^{7}\ K_{-13}^{-1}\, T_{g,1}^{-1}\, a_{m,-5}\, b_{m,-5}^{6}\, \Theta_{zz}^{2}\, h^{-2}\, (h-1)^{-1}$
t_{gas}	Gas Damping Time	$6.2 \times 10^{9}\ n_{4}^{-1}\, T_{g,1}^{-1/2}\, a_{m,-5}\, \Theta_{zz}$

[a]Time scales in seconds for an oblate, spheroidal, core-mantle grain rotating about its symmetry axis with kinetic energy $kT_g/2$. The notation "B_{-5}" means $B/10^{-5}$ G and similarly for other quantities in Gaussian cgs units. Core and mantle densities are assumed to be $\rho_c = 2.5$ g cm^{-3} and $\rho_m = \rho_c/3$. Magnetic properties χ' and K are volume averages over core plus mantle and are scaled appropriately for ordinary (non-superparamagnetic) substances. For super-paramagnetic grains, t_{lar} and t_{bar} should be reduced by a factor $\lesssim 10^5$.

REFERENCES

Aitken, D.K., Bailey, J.A., Roche, P.F., & Hough, J.H. 1985, MNRAS, 215, 815

Arfken, G. 1970, Mathematical Methods for Physicists (New York: Academic Press)

Burke, J.R., & Hollenbach, D.J. 1983, ApJ, 265, 223

Chandrasekhar, S. 1943, Rev Mod Phys, 15, 1

Cugnon, P. 1971, A&A, 12, 398

——. 1983 A&A, 120, 156

——. 1985 A&A, 152, 1

Davis, L., & Greenstein, J. 1951, ApJ, 114, 206 (DG)

DeGraff, T.A., Roberge, W.G., & Flaherty, J.E. 1993, in preparation (Paper II)

Dolginov, A.Z. & Mytrophanov, I.G. 1976, Ap. Space Sci., 43, 291

Dragovan, M. 1986, ApJ, 308, 270

Draine, B.T. 1987, Princeton Observatory Preprint No. 213

——. 1988, ApJ, 333, 848

Draine, B.T., & Lee, H.M. 1984, ApJ, 285, 89

Duley, W.W. 1978, ApJ, 219, L129

Fox R.F. 1987, J. Stat. Phys. 46, 1145

Gard, T.C. 1988, Intro. to Stochastic Differential Equations, (New York: Marcel Dekker, Inc.)

Gardiner, C.W. 1990, Handbook of Stochastic Physics, Second Edition (New York: Springer-Verlag)

Goldstein, H. 1950, Classical Mechanics (Reading, MA: Addison-Wesley)

Greenberg, J.M. 1968, in Stars and Stellar Systems, Vol. 7, Nebulae and Interstellar Matter, ed. B.M. Middlehurst & L.H. Aller (Chicago: U. of Chicago Press), p. 221

Gold, T. 1952, MNRAS, 112, 215

Harwit, M. 1970, Nature, 226, 61

Hildebrand, R.H. 1988a, Astro. Lett. and Communications, 26, 263

Hildebrand, R.H. 1988b, Quart. JRAS, 29, 327

——. 1989, in IAU Symp. 135, Interstellar Dust, ed. L.J. Allamandola & A.G.G.M. Tielens (Dordrecht: Reidel), p. 275

Hildebrand, R.H., Gonatas, D.P., Platt, S.R., Wu, X.D., Davidson, J.A., Werner, M.W., Novak, G., & Morris, M. 1990, ApJ, 362, 114

Hildebrand, R.H., Davidson, J.A., Dotson, J., Figer, D.F., Novak, G., Platt, S.R., & Tao, L. 1992, preprint

Johnson, P. E. 1982, Nature, 295, 371

Johnson, P. E., Rieke, G.H., Lebofsky, M.J., & Kemp, J.C. 1981, ApJ, 245, 671

Jones, R.V., & Spitzer, L. (Jr.) 1967, ApJ, 147, 943 (JS67)

Jones, T.J., Hyland, A.R., & Bailey, J. 1984, ApJ, 282, 675

Lee, H.M., & Draine, B.T. 1985, ApJ, 290, 211

Martin, P.G. 1971, MNRAS, 153, 279

Martin, P.G., & Whittet, D.C.B.W. 1990, 357, 113

Press, W.H., Flannery, B.P., Teukolsky, S.A., & Vetterling, W.T. 1986, Numerical Recipes (Cambridge, UK: Cambridge U. Press)

Purcell, E.M. 1969, Physica, 41, 100

——. 1979, ApJ, 231, 404 (P79)

Purcell, E.M., & Spitzer, L. (Jr.) 1971, ApJ, 167, 31 (PS71)

Reichl, L.E. 1980, A Modern Course in Statistical Physics (Austin: U. Texas Press)

Roberge, W.G., & Hanany, S. 1993, in preparation

Spitzer, L. (Jr.) 1978, Physical Processes in the Interstellar Medium (New York: Wiley)

Spitzer, L. (Jr.), & Tukey, J.W. 1951, ApJ, 114, 187

Spitzer, L. (Jr.), & McGlynn, T.A. 1979, ApJ, 231, 417

Tamura, M., Nagata, T., Sato, S., & Tanaka, M. 1987, MNRAS, 224, 413

Tielens, A.G.G.M., & Allamandola, L.J. 1987, in Physical Processes in Interstellar Clouds, ed. D.J. Hollenbach & H.A. Thronson Jr. (Dordrecht: D. Reidel) p. 397

van de Hulst, H.C. 1981, Light Scattering by Small Particles, (New York: Dover)

Werner, M.W., Davidson, J.A., Morris, M., Novak, G., Platt, S.R., & Hildebrand, R.H. 1988, ApJ, 333, 729

Whittet, D.C.B. 1992, Dust in the Galactic Environment (Bristol, UK: Inst. of Physics Publishers)

Wilking, B.A., Lebofsky, M.J., Martin, P.G., Rieke, G.H., & Kemp, J.C. 1980, ApJ, 235, 905

Wilking, B.A., Lebofsky, M.J., Rieke, G.H. 1982, AJ, 87, 695

FIGURE CAPTIONS

Fig. 1 — Relationship betwee the basis vectors $(\hat{x}, \hat{y}, \hat{z})$ of the gas frame and $\left(\hat{x}^b, \hat{y}^b, \hat{z}^b\right)$ of the body frame. The transformation of vectors and tensors between the two frames depends on the Eulerian angles, β, ϕ, and ψ.

Fig. 2 — Eccentricity factors, $\Gamma_\perp$ and $\Gamma_{||}$, defined by eq. (3.34)–(3.35), plotted vs. the mantle eccentricity. The efficiency of grain alignment by collisions, evaporation, plus paramagnetic absorption (§4) depends on grain shape only via the ratio $\Gamma_\perp/\Gamma_{||}$, which is also plotted.

Fig. 3 — Photoabsorption damping time, eq. (3.58), for silicate grains immersed in a thermal radiation bath with temperature T_{rad}. For simplicity we consider bare silicate grains with density $\rho_c = 2.5$ g cm^{-3} and axis ratios of 1:1 (solid), 2:1 (long dash), and 5:1 (short dash). In each case we consider three radii, $b_c = 0.02$, 0.1, and 0.5 μm. The largest and smallest damping time for each axis ratio correspond, respectively to the largest and smallest radius.

Fig. 4 — Similar to Fig. 3, but the quantity plotted is the photoemission damping time, eq. (3.67).

Fig. 5 — Symbols: Root-mean-square value of the relative errors in $\langle\cos^2\beta\rangle$ obtained from 50 identical trial calculations for spherical grains. E_{rms} is plotted as a function of τ_{avg}/τ_{cor}, the averaging time in units of the correlation time. All calculations pertain to spheres with $T_d/T_g = 0.5$, $\delta = 1$ and used a dimensionless time step of $\Delta\tau/\tau_{cor} = 1 \times 10^{-3}$. Solid curve: Least squares fit of a straight line to the symbols. The line has slope -0.47.

Fig. 6 — Similar to Fig. 5, but E_{rms} is plotted as a function of the integration step size in units of the correlation time. All other parameters have values as in Fig. 5, except that the averaging time is $5 \times 10^4 \tau_{cor}$.

Fig. 7 — Histogram: Distribution of the relative errors in $\langle\cos^2\beta\rangle$ for 100 trials with $\Delta\tau/\tau_{cor} = 1 \times 10^{-3}$ and $\tau_{avg}/\tau_{cor} = 6 \times 10^4$. All calculations pertain to spheres with

$T_d/T_g = 0.9$ and $\delta = 3$. The plotted error distribution has mean value $\overline{E}_{rms} = -1.1 \times 10^{-3}$ and standard deviation $\sigma_E = 5.1 \times 10^{-3}$. Dashed curve: Gaussian distribution with zero mean, standard deviation equal to σ_E, and normalization chosen to have the same area as the histogram.

Fig. 8 — Similar to Fig. 7, but the averaging time for each trial is $\tau_{avg}/\tau_{cor} = 1 \times 10^6$. The error distribution indicated by the histogram has mean value $\overline{E}_{rms} = -5.8 \times 10^{-6}$ and standard deviation $\sigma_E = 1.3 \times 10^{-3}$.

Fig. 9 — Rayleigh reduction factor for spherical grains plotted vs. δ. Symbols: Numerical results obtained by integrating the Langevin equation with $\Delta\tau/\tau_{cor} = 1 \times 10^{-3}$ and $\tau_{avg}/\tau_{cor} = 5 \times 10^4$. Solid curves: Exact solution for spheres obtained from eq. (4.14). The root-mean square relative error in the numerical values of R (not $\log R$) is 1.3%. Notice that the relative errors are larger for small R-values because $\langle \cos^2 \beta \rangle \to 1/3$ as $R \to 0$ (cf. eq. [1.1]).

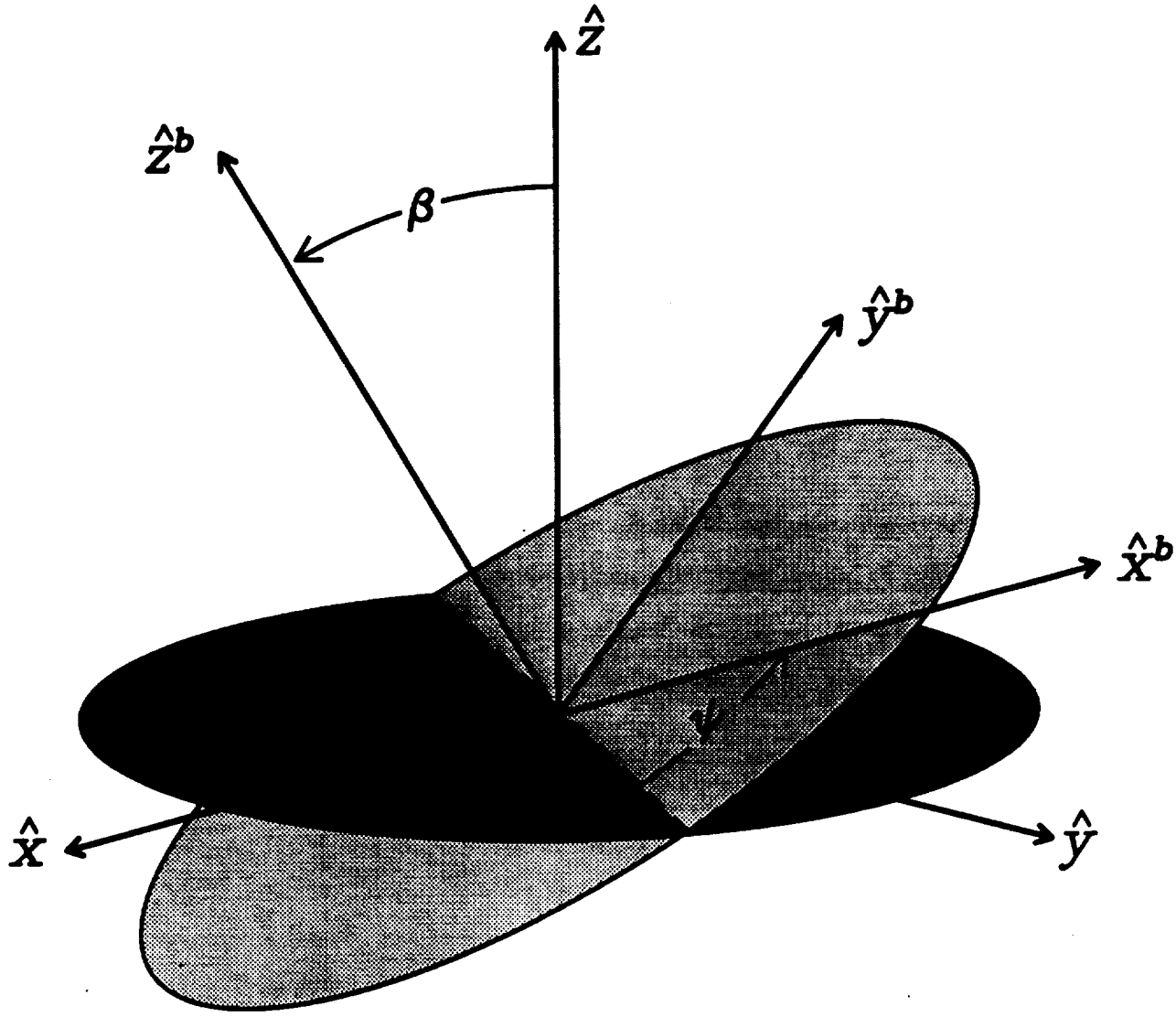

Fig. 1

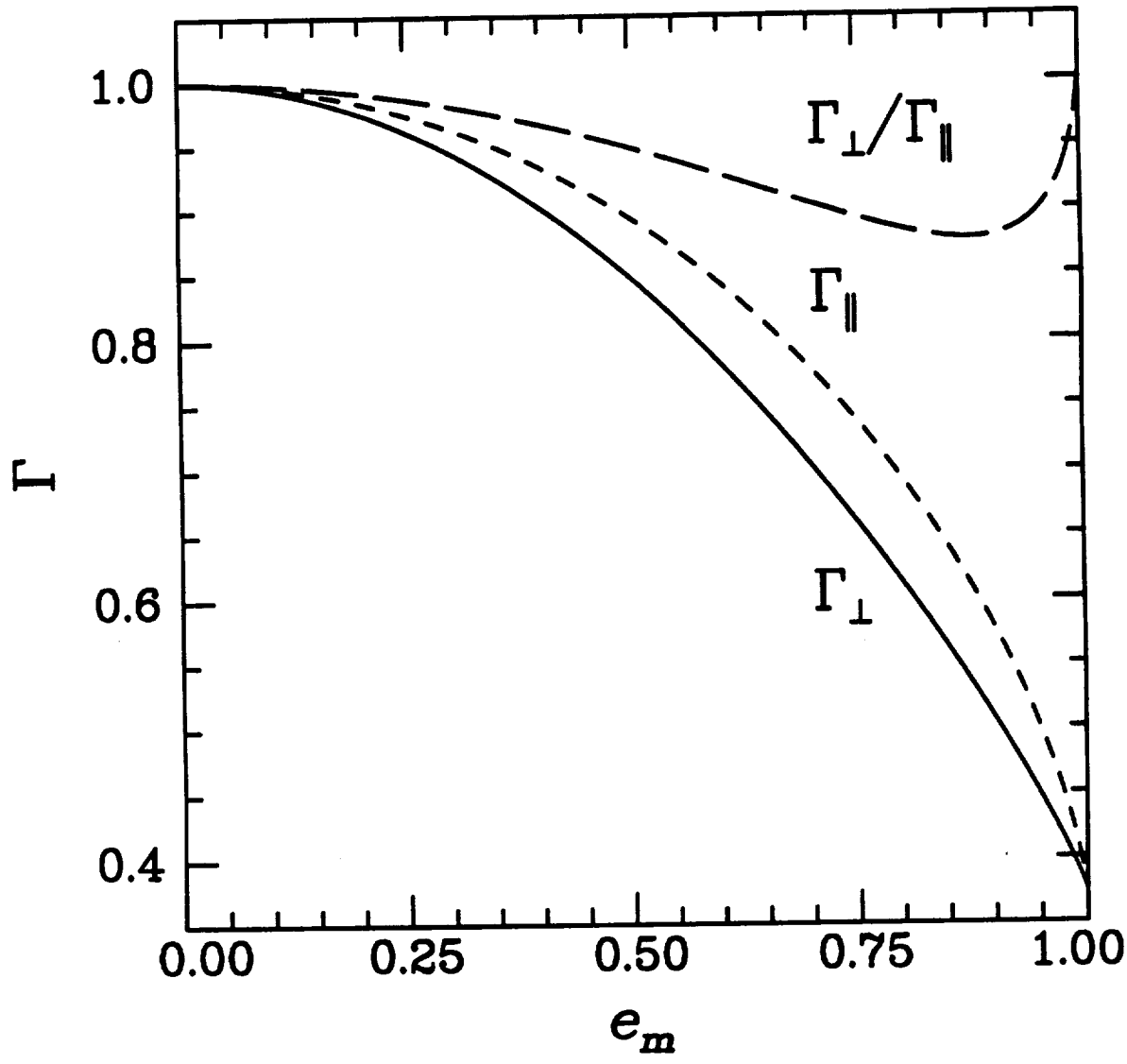
1.0
0.8
0.6
0.4
Γ
0.00
0.25
0.50
0.75
1.00
e_m
$\Gamma_\perp/\Gamma_\parallel$
$\Gamma_\parallel$
$\Gamma_\perp$

Fig. 2

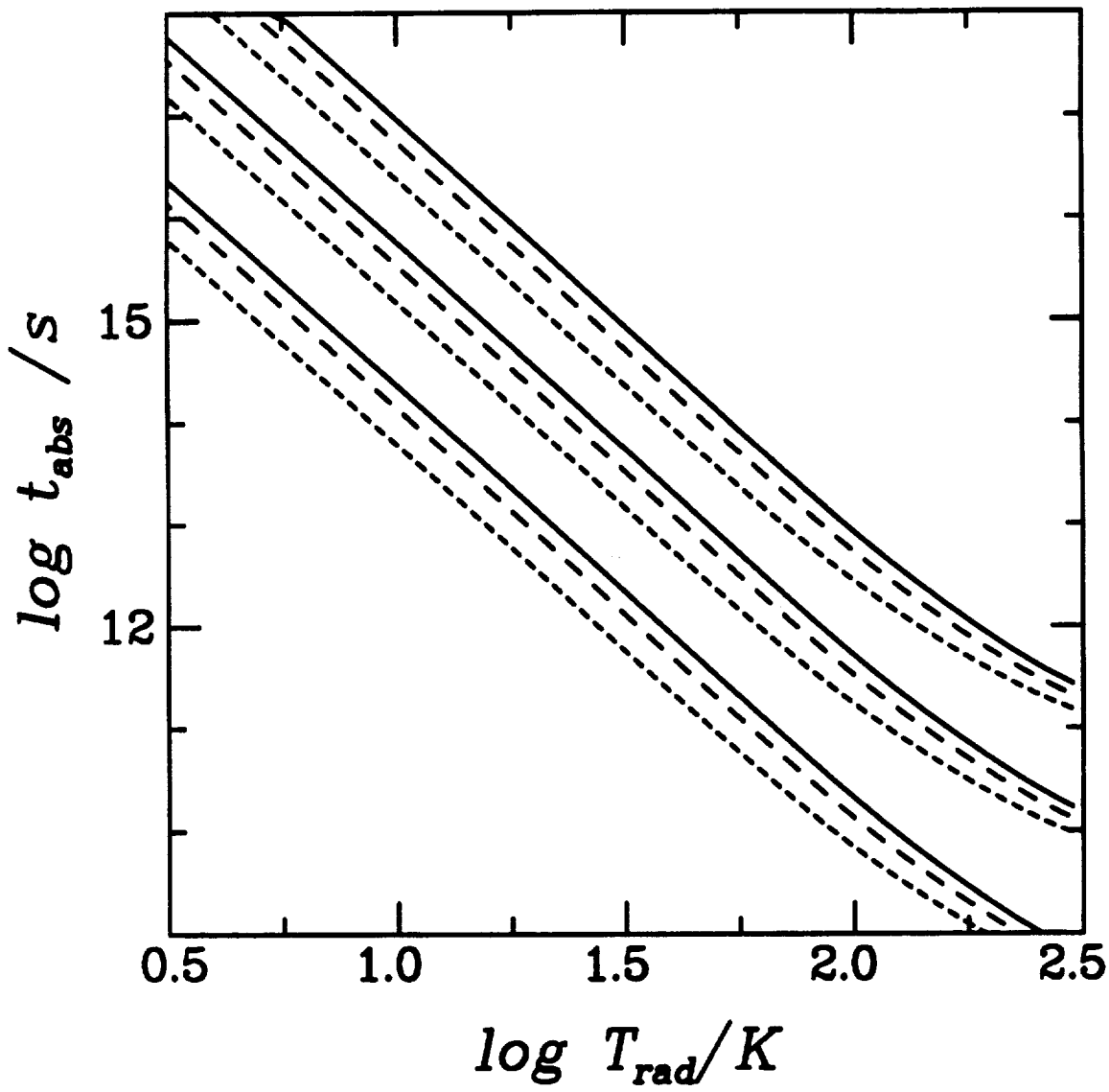

Fig. 3

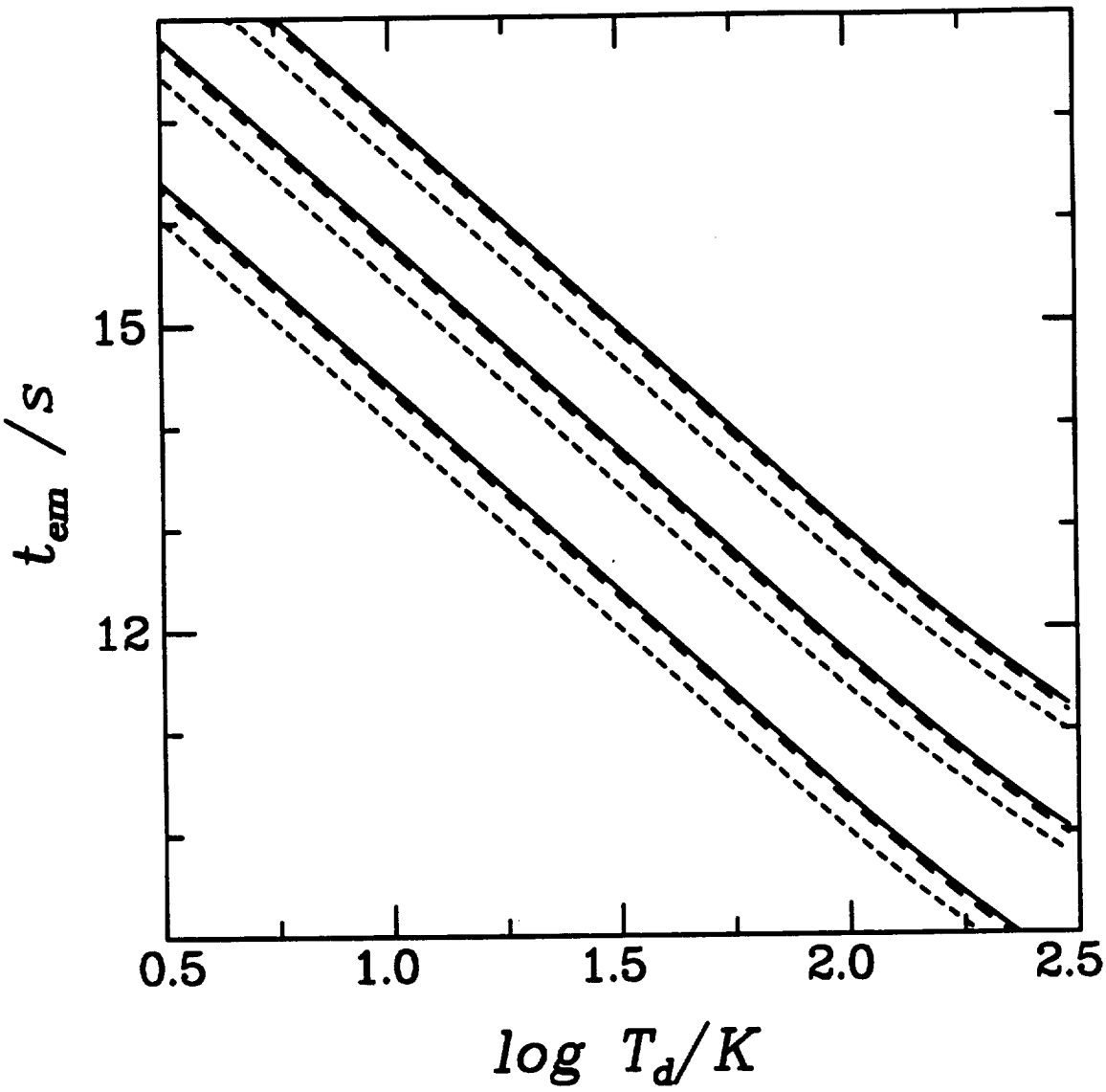

Fig. 4

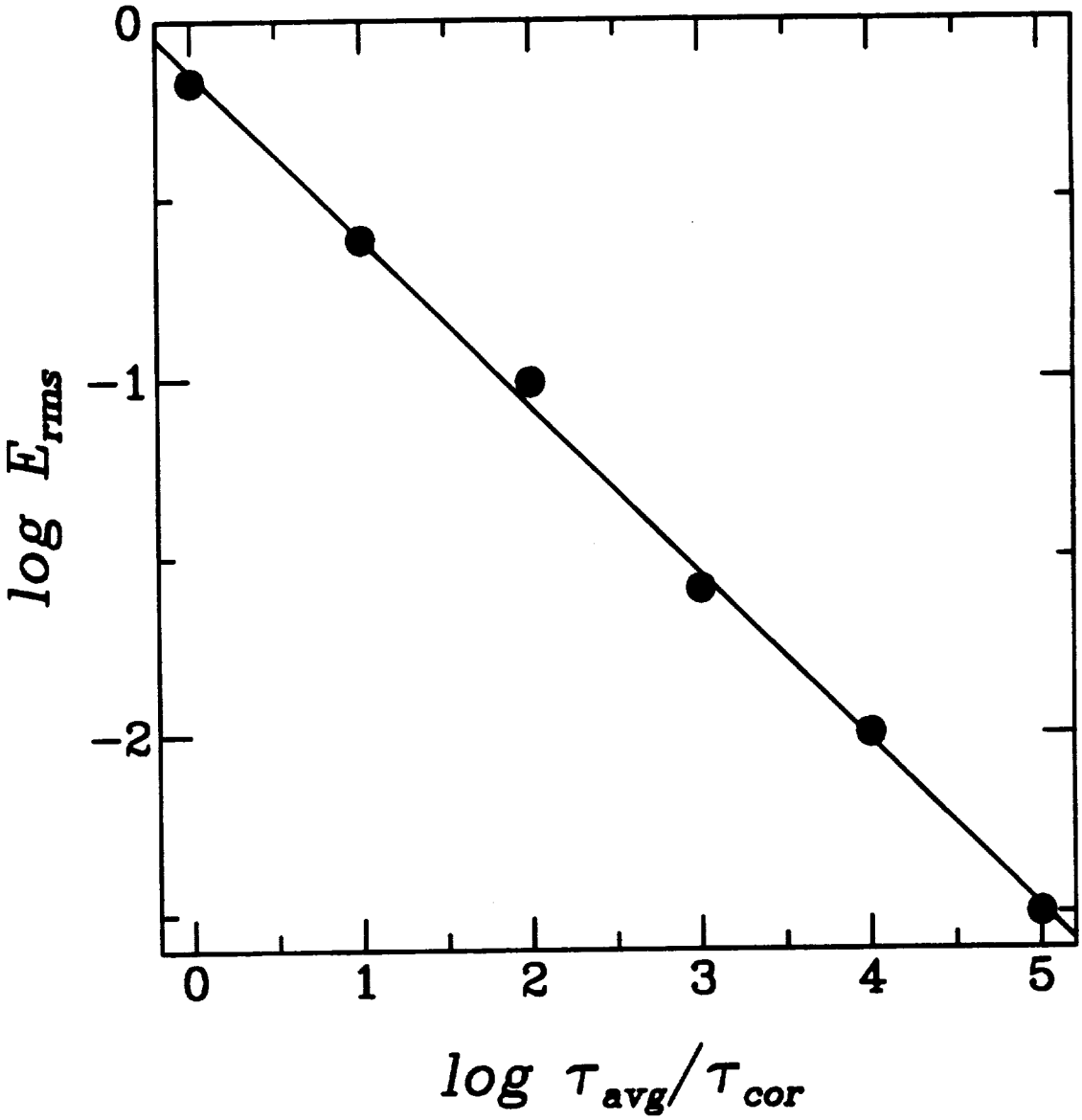

Fig. 5

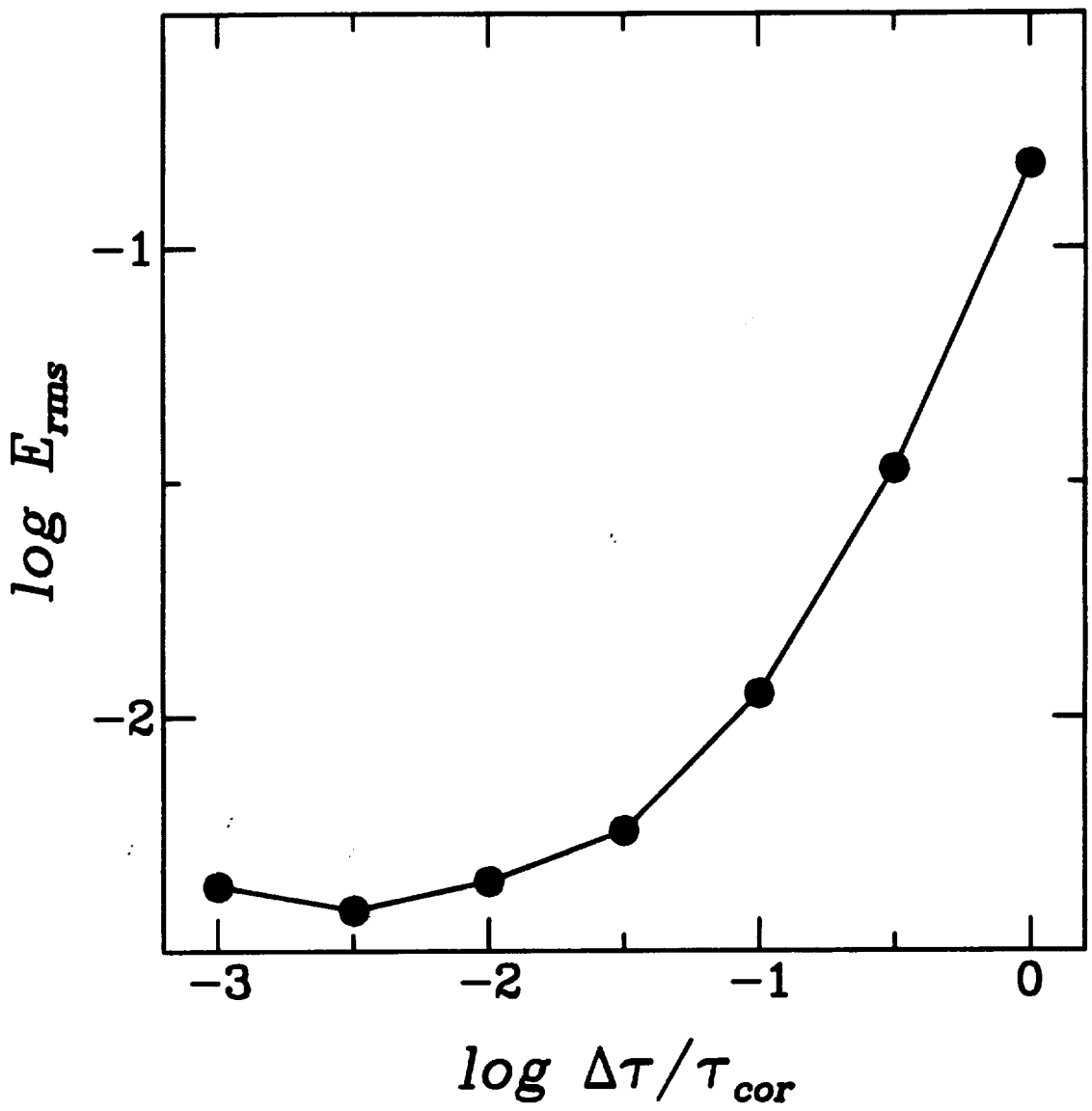

Fig. 6

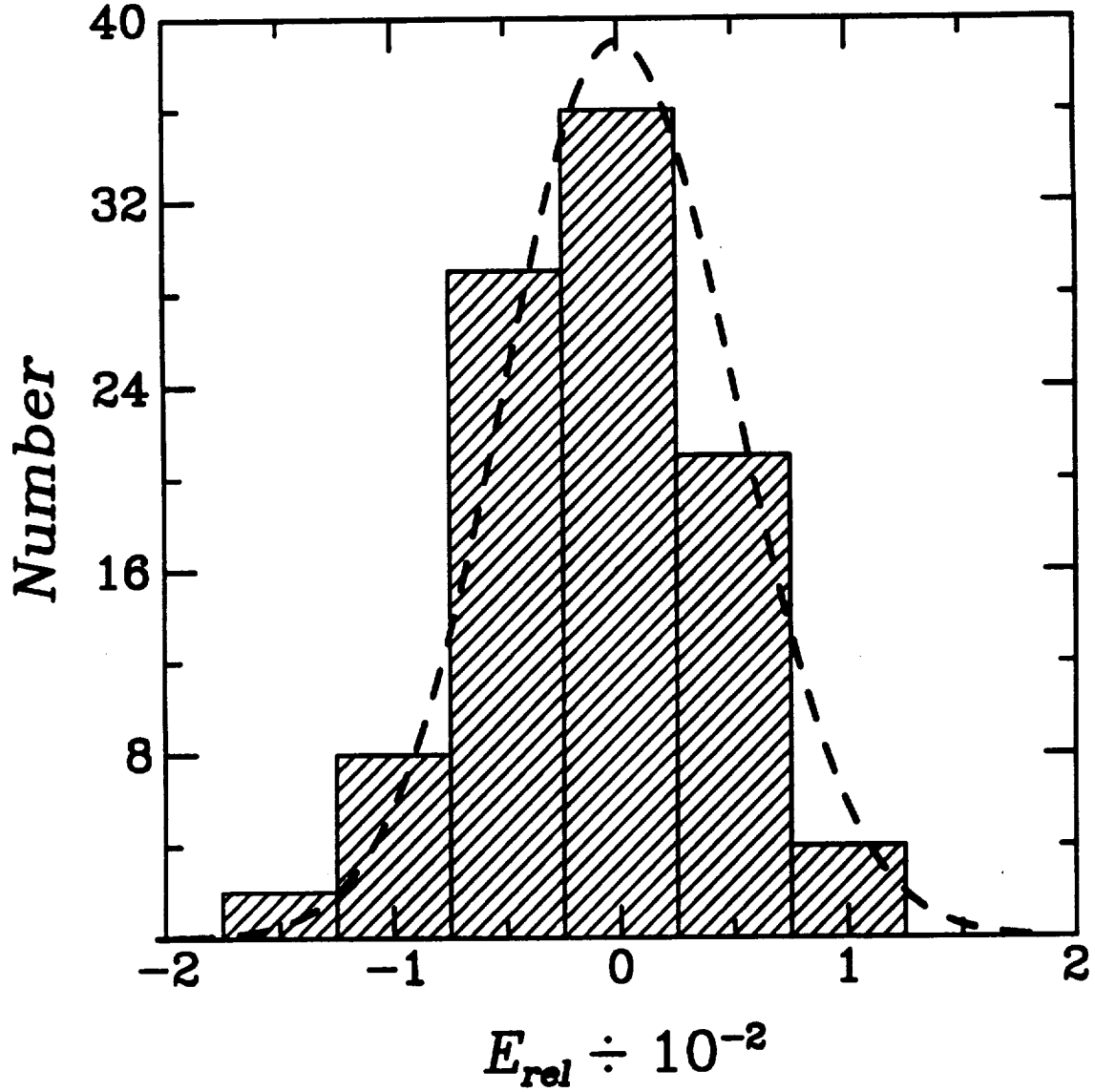

Fig 7

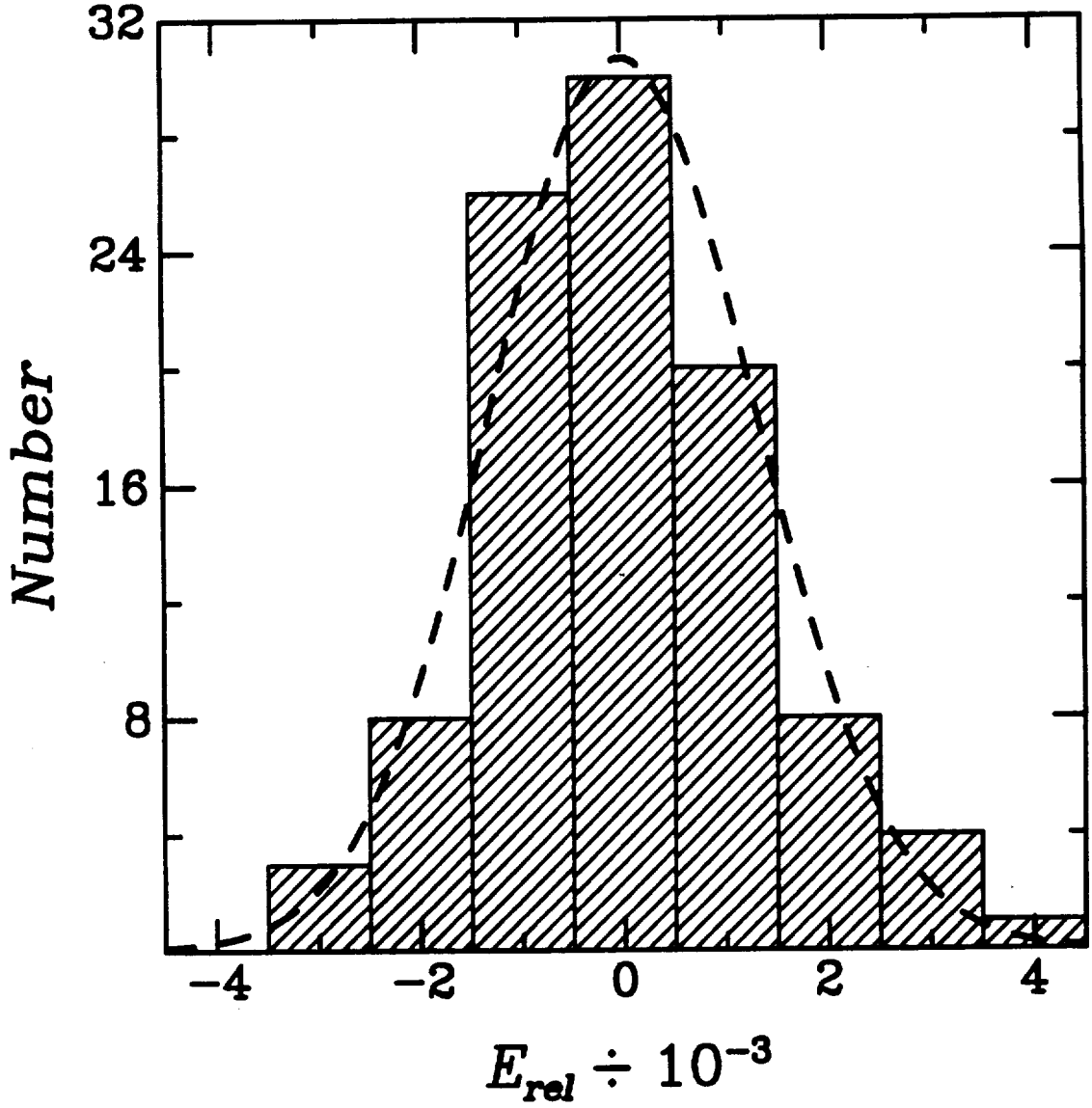

Fig 8

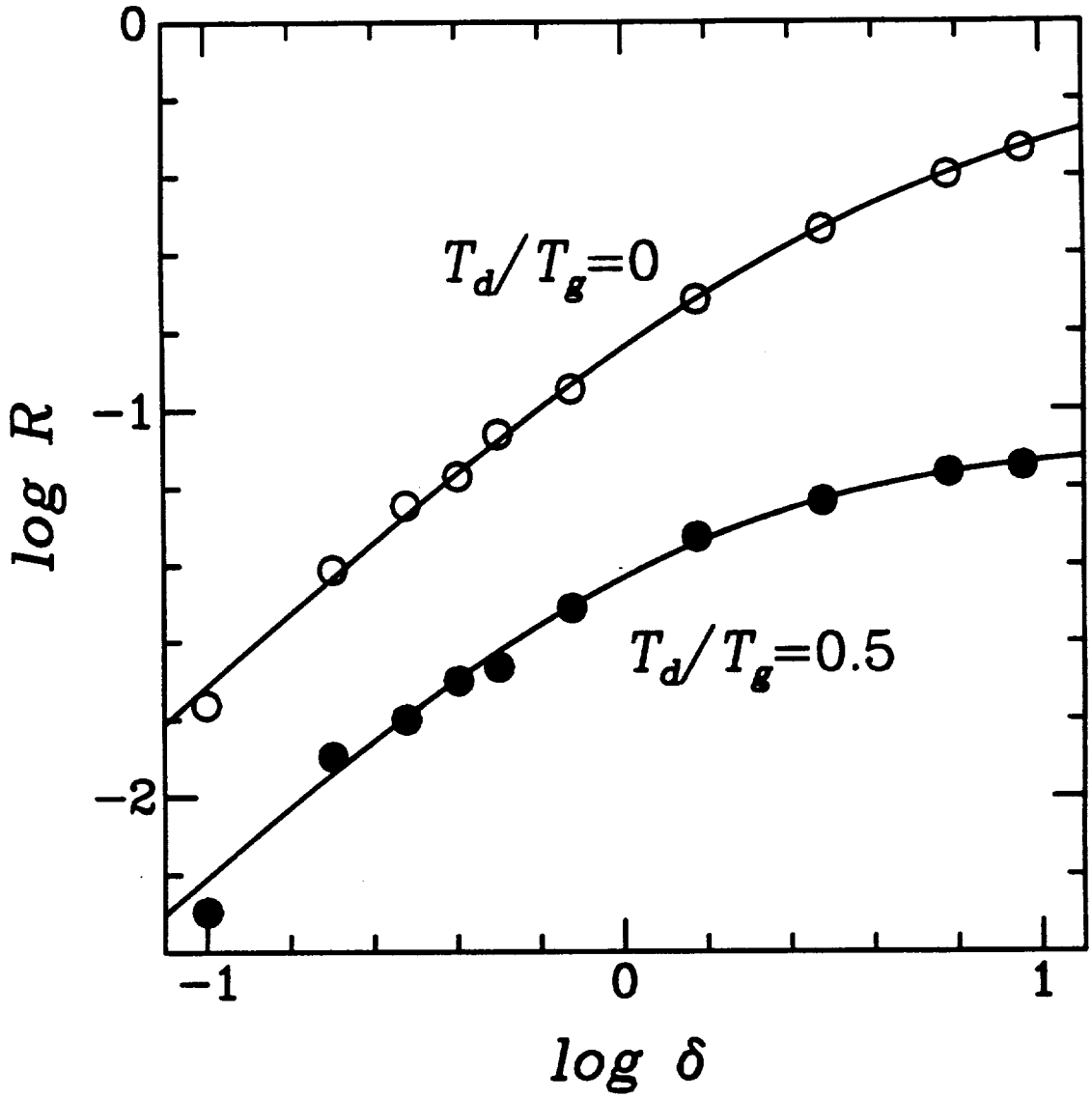

Fig. 9